TESIS DOCTORAL

Translational steps towards the clinical application of TAT-Cx43$_{266-283}$ for the treatment of glioblastoma

EGFR as a predictor and mediator of treatment response, and positive results in combination with tumor resection in a preclinical model

Andrea Álvarez Vázquez

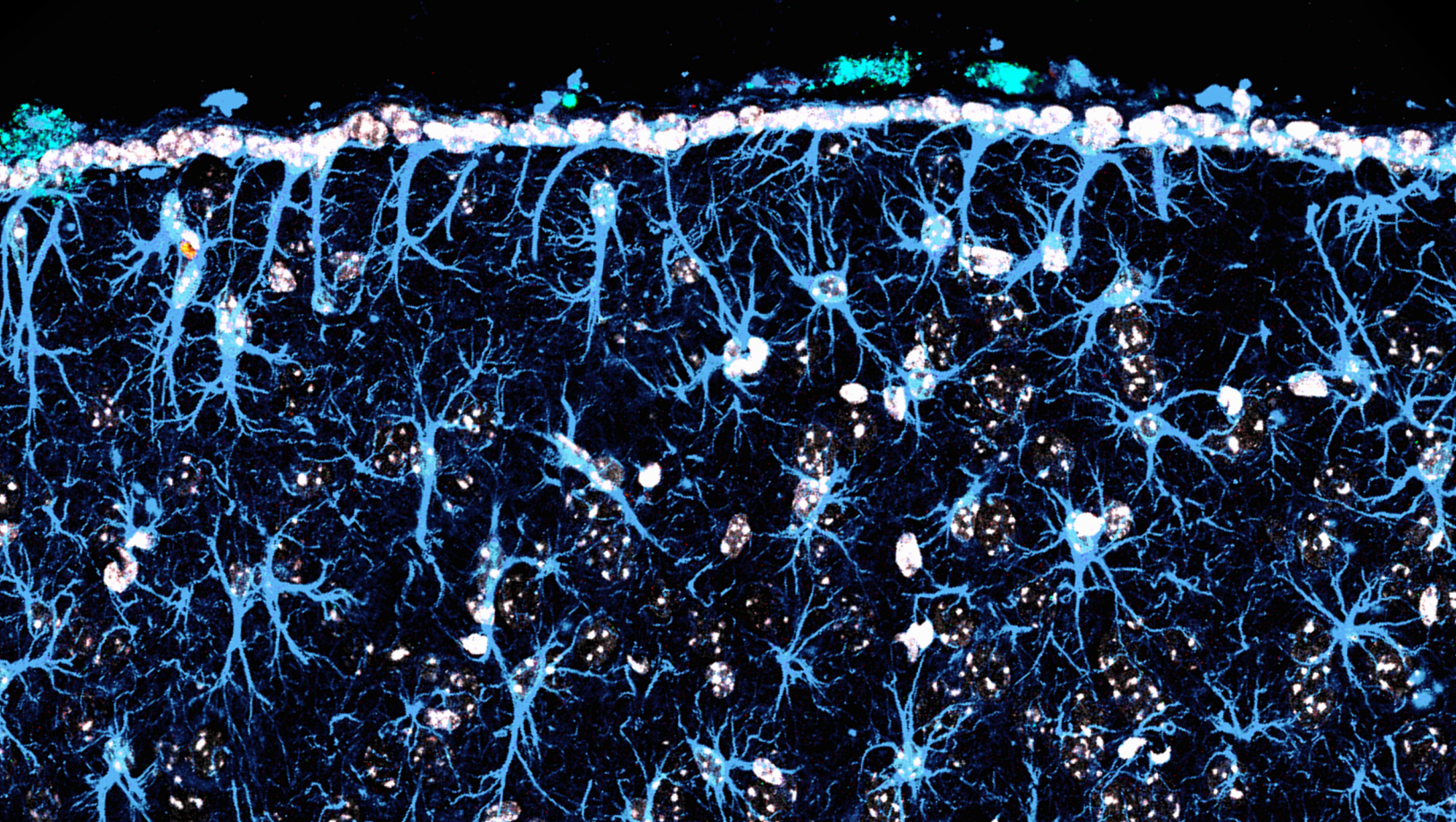

PHD THESIS

Translational steps towards the clinical application of TAT-Cx43$_{266-283}$ for the treatment of glioblastoma

EGFR as a predictor and mediator of treatment response, and positive results in combination with tumor resection in a preclinical model

Andrea Álvarez Vázquez

Universidad de Salamanca

2023

Directora/Supervisor: Aránzazu Tabernero Urbieta

VNiVERSiDAD D SALAMANCA
CAMPUS DE EXCELENCIA INTERNACIONAL

800 AÑOS
1218 - 2018

INSTITUTO DE NEUROCIENCIAS CASTILLA Y LEON

INSTITUTO DE NEUROCIENCIAS DE CASTILLA Y LEÓN (INCYL)
Neurobiochemistry

Dª ARÁNZAZU TABERNERO URBIETA, Catedrática de Bioquímica y Biología Molecular de la Universidad de Salamanca.

AUTORIZA:

La presentación de la Tesis Doctoral titulada "Translational steps towards the clinical application of TAT-Cx43$_{266-283}$ for the treatment of glioblastoma: EGFR as a predictor and mediator of treatment response, and positive results in combination with tumor resection in a preclinical model", realizada baja su dirección por Dª Andrea Álvarez Vázquez en el Programa de Doctorado de Neurociencias del Instituto de Neurociencias de Castilla y León y Departamento de Bioquímica y Biología Molecular, de la Universidad de Salamanca. Además, considera que esta Tesis reúne los requisitos, calidad y rigor científico necesarios para que Dª Andrea Álvarez Vázquez opte al grado de Doctora en Neurociencias con Mención Internacional por la Universidad de Salamanca.

Y para que así conste firma el siguiente documento en Salamanca a 20 de Diciembre de 2023.

TABERNERO URBIETA MARIA ARANZAZU - 07863000J

Firmado digitalmente por TABERNERO URBIETA MARIA ARANZAZU - 07863000J
Fecha: 2023.12.20 22:29:06 +01'00'

Fdo. Aránzazu Tabernero Urbieta

Arantxa Tabernero – lab 15. Instituto de Neurociencias de Castilla y León (INCYL). *Universidad de Salamanca* -37007 Salamanca Spain -Teléf.: 923 294500 ext: 5311 -Email: ataber@usal.es

VNiVERSiDAD D SALAMANCA
CAMPUS DE EXCELENCIA INTERNACIONAL

800 AÑOS
1218 ~ 2018

ESCUELA DE DOCTORADO
EDIFICIO MULTIUSOS I+D+I
C/ ESPEJO Nº 2 – 1ª PLANTA. 37007 SALAMANCA

IMPRIMIR RESTABLECER

SOLICITUD DE AUTORIZACIÓN DE ESTANCIA PARA LA OBTENCIÓN DE LA MENCIÓN INTERNACIONAL

NOMBRE Y APELLIDOS DEL DOCTORANDO Andrea Álvarez Vázquez

PROGRAMA DE DOCTORADO Neurociencias

INSTITUCIÓN DONDE SE REALIZARÁ LA ESTANCIA

Cleveland Clinic Lerner Research Institute

FECHAS DE REALIZACIÓN DE LA ESTANCIA 07/09/2022-06/12/2022

NOMBRE Y APELLIDOS DEL DIRECTOR/A(S) DE LA TESIS

Aránzazu Tabernero Urbieta

INFORME DEL DIRECTOR DE LA TESIS QUE AVALA LA ESTANCIA

La tesis de Andrea Álvarez tiene como objetivo el acercar la administración del péptido antitumoral TAT-Cx43 266-283 a la clínica. La primera terapia administrada a los pacientes con glioblastoma es la resección quirúrgica del tumor, por lo que uno de los objetivos de la tesis será la combinación de la resección con la administración del péptido. Para ello, Andrea realizará una estancia en el laboratorio del Dr. Justin Lathia en el Cleveland Clinic Lerner Research Institute, un laboratorio altamente traslacional por su situación única dentro de un hospital como el Cleveland Clinic. Este laboratorio cuenta con la experiencia de una neurocirujana que dispone de un modelo de ratón de resección quirúrgica que Andrea aprenderá para finalmente combinar dicha terapia con la administración del péptido TAT-Cx43 266-283, promoviendo así su desarrollo hacia un contexto más clínico.

FIRMA DEL DIRECTOR/A (S) DE LA TESIS

La Comisión Académica del Programa de Doctorado, reunida en sesion el día _____ acordó autorizar la presente solicitud.

El/la Presidente/a de la Comisión Académica

TABERNERO URBIETA MARIA ARANZAZU - 07863000J

Firmado digitalmente por TABERNERO URBIETA MARIA ARANZAZU - 07863000J
Fecha: 2022.12.20 20:49:01 +01'00'

Fdo: _____

COMISIÓN ACADÉMICA DEL PROGRAMA DE DOCTORADO

Cleveland Clinic
Lerner Research Institute

Justin D. Lathia, PhD
Professor and Vice Chair
Department of Cardiovascular & Metabolic Sciences
Director for Faculty Development
Lerner Research Institute, Cleveland Clinic

Scientific Director and Melvin H. Burkhardt Endowed Chair in Neuro-Oncology; Rose Ella Burkhardt Brain Tumor & Neuro-Oncology Center, Cleveland Clinic

Reza Khatib MD Professor
Co-Leader, Molecular Oncology Program
Case Comprehensive Cancer Center

9500 Euclid Ave, NE3-202
Cleveland, OH 44195
Phone: (216) 445-7475
lathiaj@ccf.org

December 15, 2023

Re: Letter of stay confirmation for Andrea Álvarez Vázquez

To whom it may concern,

This letter is to confirm that we hosted Andrea Álvarez Vázquez in my laboratory at the Cleveland Clinic, Lerner Research Institute (Cleveland, OH, U.S.A.) to perform a 3 month-research stay under my supervision, from September 7th 2022 – December 6th 2022. During this time period, she worked on several projects involving our mutual interests in targeting malignant brain tumors. As a result of this collaboration, there are several manuscript that are being prepared to disclose the results of these findings.

Please do not hesitate to contact me should you have any additional questions.

Sincerely,

Justin D. Lathia

Justin Lathia, PhD

Abbreviations

ANOVA	Analysis of variance
AP	Anterior-posterior
BBB	Blood-brain barrier
BBTB	Blood-brain-tumor barrier
b-FGF	Basic fibroblast growth factor
BMP-4	Bone morphogenic protein 4
BSA	Bovine serum albumin
CNS	Central nervous system
CSK	C-terminal Src kinase
CX	Connexin
DAPI	4′,6-diamidino-2-phenylindole
DCX	Doublecortin
DMSO	Dimethyl sulfoxide
DNA	Deoxyribonucleic acid
EDTA	Ethylene-diamine-tetra-acetic acid
EGF	Epidermal growth factor
EGFR	Epidermal growth factor receptor
EGTA	Ethylene-glycol-tetra-acetic acid
FAK	Focal adhesion kinase
FBS	Fetal bovine serum
FISH	Fluorescence in situ hybridization
GAPDH	Glyceraldehyde-3-phosphate dehydrogenase
GBM	Glioblastoma
GFAP	Glial Fibrillary Acidic Protein
GFP	Green Fluorescent Protein

GSC	Glioblastoma stem cell
H&E	Hematoxylin-eosin
HRP	Horseradish peroxidase
IDH	Isocitrate dehydrogenase
IgG	Immunoglobulin G
IVIS	In vivo imaging system
LM	Lateral-medial
MTT	3-(4,5-dimethylthiazol-2-yl)-2,5-diphenyltetrazolium bromide
NF1	Neurofibromatosis type 1
NGS	Normal goat serum
NPC	Neural progenitor cell
NSC	Neural stem cell
OPC	Oligodendrocyte progenitor cell
PBS	Phosphate buffered saline
PCR	Polymerase chain reaction
PDGFRA	Platelet-derived growth factor receptor alpha
PFA	Paraformaldehyde
PTEN	Phosphatase and tensin homolog
RNA	Ribonucleic acid
ROI	Region of interest
RPPA	Reverse-phase protein array
SDS	Sodium dodecyl sulfate
SEM	Standard error of the mean
SFK	Src family kinase
SH3	Src homology domain 3
SVZ	Subventricular zone
TCGA	The Cancer Genome Atlas
TERT	Telomerase reverse transcriptase
TGFα	Transforming growth factor alpha

TME	Tumor microenvironment
TMZ	Temozolomide
VEGF	Vascular endothelial growth factor
WB	Western blot
WHO	World Health Organization

Index

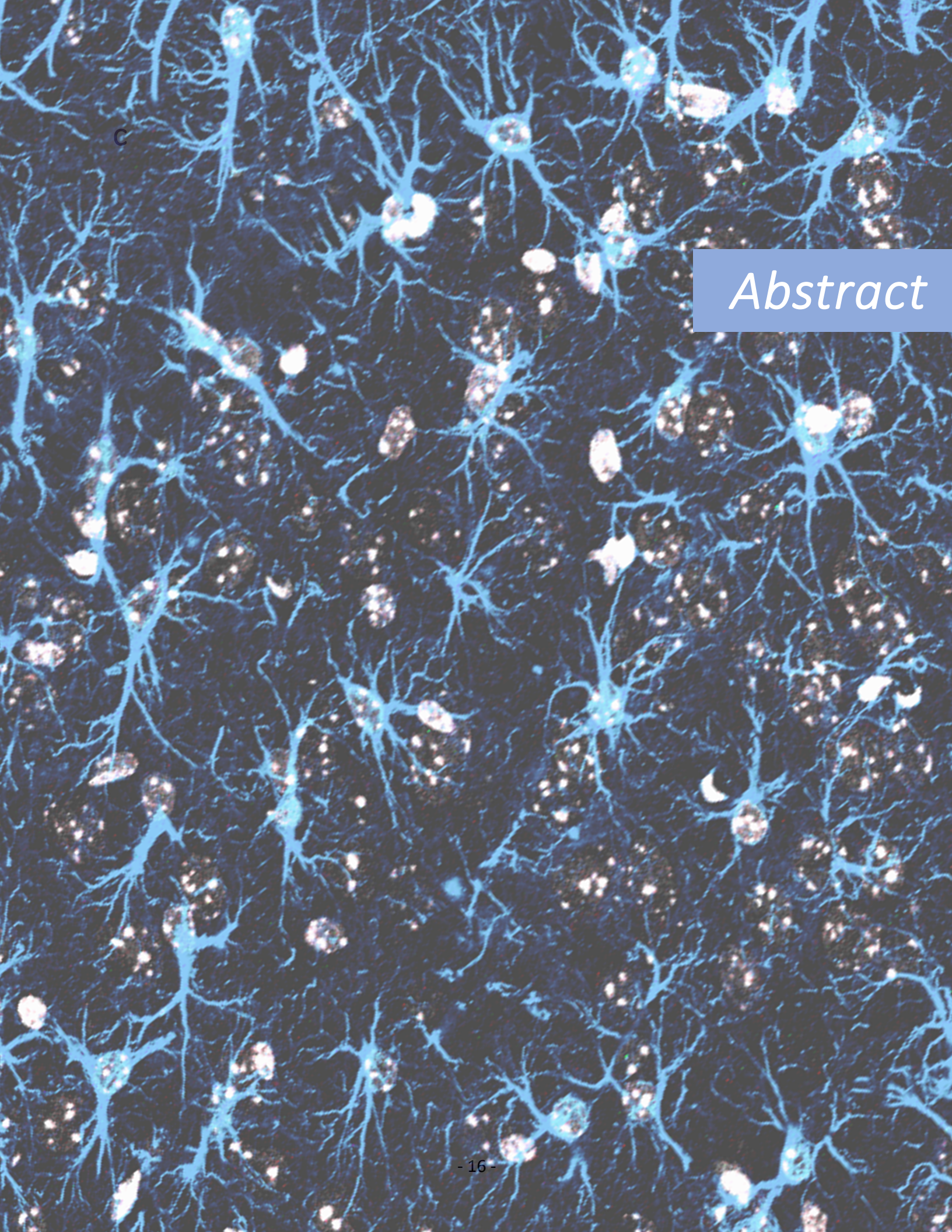

Abstract

Abstract

Glioblastomas (GBM) are the most malignant primary brain tumors and they remain incurable. Despite the current standard of care, which involves surgical resection of the tumor and adjuvant administration of chemotherapy and radiotherapy, some GBM stem cells (GSCs) stay in the brain parenchyma becoming one of the primary causes of tumor recurrence. Importantly, the Src-inhibitory peptide TAT-Cx43$_{266\text{-}283\ has}$ shown promising anti-tumor results in GBM preclinical models, reducing GSC viability and increasing survival in GBM-bearing mice. However, being aware of the many obstacles to overcome when translating preclinical results into a clinical setting, we have investigated some of these main gaps in order to promote the progress of TAT-Cx43$_{266\text{-}283}$ as a new clinical therapy to fight GBM.

First, we investigated biomarkers of treatment response in order to design a more targeted therapeutic approach in potential clinical applications. For that purpose, we assessed cell viability after treatment with TAT-Cx43$_{266\text{-}283}$, in a set of 13 patient-derived GSC lines. Interestingly, we found a stronger treatment response in those patient GSCs that had alterations in the Epidermal Growth Factor Receptor (EGFR) (EGFR amplification or EGFRvIII mutation). Additionally, analyzing GBM patient databases, we found a correlation between EGFR alterations and a higher Src activity, as well as worse survival outcomes. The role of EGFR as a treatment-response biomarker were confirmed in 6 murine GBM lines with and without EGFR alterations. Importantly, we found that treatment with TAT-Cx43$_{266\text{-}283}$ was more effective than the standard-of-care chemotherapeutic temozolomide (TMZ) or the classical EGFR inhibitor, erlotinib, in our murine and human GSC models. Moreover, we identified EGFR as an additional participant in TAT-Cx43$_{266\text{-}283}$ response together with Src, as shown by the decrease in EGFR and EGFRvIII activity observed in some GSCs and the increased survival upon TAT-Cx43$_{266\text{-}283}$-administration in a mouse model in which tumors were generated by NSCs with EGFR and other glioma-driver mutations (NPE-IE cells).

Next, we studied the effect of TAT-Cx43$_{266\text{-}283}$ in a clinical context by administering the treatment in a murine model of tumor resection. We additionally analyzed the histopathology of this GBM model, uncovering histological features typical of human GBM, such as necrosis, invasive borders, and the presence of multiple proliferative spread foci outside the primary tumor mass. We found that resection alone improved, although not significantly, GBM-bearing mice survival. However, tumors that regrew after resection exhibited more aggressive features. Importantly, the combination of tumor resection and TAT-Cx43$_{266\text{-}283}$ achieved better survival outcomes and showed reduced invasive features.

Altogether, these results serve as a base for future clinical investigations and, together with previous studies, support the therapeutic potential of TAT-Cx43$_{266\text{-}283}$ as a treatment for GBM.

Resumen

Los glioblastomas (GBM) son los tumores cerebrales primarios más malignos y, actualmente, siguen siendo incurables. A pesar del tratamiento estándar actual, que implica la resección quirúrgica del tumor y la administración adyuvante de quimioterapia y radioterapia, algunas células madre de GBM (GSCs) permanecen en el parénquima cerebral, convirtiéndose en una de las principales causas de recurrencia del tumor. Cabe destacar que el péptido inhibidor de Src TAT-Cx43$_{266-283}$ ha mostrado resultados antitumorales prometedores en modelos preclínicos de GBM, reduciendo la viabilidad de las GSCs y aumentando la supervivencia en modelos murinos de GBM. Sin embargo, puesto que somos conscientes de los numerosos obstáculos que hay que superar para trasladar los resultados preclínicos al ámbito clínico, hemos investigado algunas de estas barreras, con el fin de promover el progreso de TAT-Cx43$_{266-283}$ como nueva terapia clínica para combatir el GBM.

En primer lugar, investigamos biomarcadores de respuesta al tratamiento, con el fin de diseñar un enfoque terapéutico más específico en potenciales aplicaciones clínicas. Para ello, evaluamos la viabilidad celular tras el tratamiento con TAT-Cx43$_{266-283}$ en un conjunto de 13 líneas de GSC derivadas de pacientes. Curiosamente, encontramos una mayor respuesta al tratamiento en aquellas GSCs de pacientes que presentaban alteraciones en el Receptor del Factor de Crecimiento Epidérmico (EGFR) (amplificación del EGFR o mutación EGFRvIII). Además, analizando bases de datos de pacientes con GBM, encontramos una correlación entre las alteraciones de EGFR y una mayor actividad Src, así como peores resultados de supervivencia. El papel de EGFR como biomarcador de respuesta al tratamiento se confirmó en 6 líneas murinas de GBM con y sin alteraciones de EGFR. Es importante destacar que el tratamiento con TAT-Cx43$_{266-283}$ fue más eficaz que la quimioterapia estándar con temozolomida (TMZ) o el inhibidor clásico de EGFR, erlotinib, en nuestros modelos in vitro de GSC murinas y humanas. Además, identificamos a EGFR como un participante adicional en la respuesta a TAT-Cx43$_{266-283}$ junto con Src, como lo demuestra la disminución de la actividad del EGFR y del EGFRvIII observada en algunas GSCs tratadas, y el aumento de la supervivencia tras la administración de TAT-Cx43$_{266-283}$ en un modelo de ratón en el que los tumores fueron generados por NSCs con EGFR y otras mutaciones generadoras de glioma (células NPE-IE).

A continuación, estudiamos el efecto de TAT-Cx43$_{266-283}$ en un contexto más clínico administrando el tratamiento en un modelo murino de resección tumoral. Además, analizamos la histopatología de este modelo de GBM, descubriendo características histológicas típicas del GBM humano, como necrosis, bordes invasivos y la presencia de múltiples focos proliferativos diseminados fuera de la masa tumoral primaria. Descubrimos que la resección por sí sola podía mejorar, aunque no significativamente, la supervivencia de los ratones portadores de GBM. Sin embargo, los tumores que volvían a crecer tras la resección mostraban características más agresivas. Es importante destacar que la combinación de resección tumoral y TAT-Cx43$_{266-283}$ logró los mejores datos de supervivencia de los ratones con GBM, así como una reducción de la invasividad de dichos tumores.

En conjunto, estos resultados sirven de base para futuras investigaciones clínicas y, junto con estudios anteriores, apoyan el potencial terapéutico de TAT-Cx43$_{266-283}$ como tratamiento para el GBM.

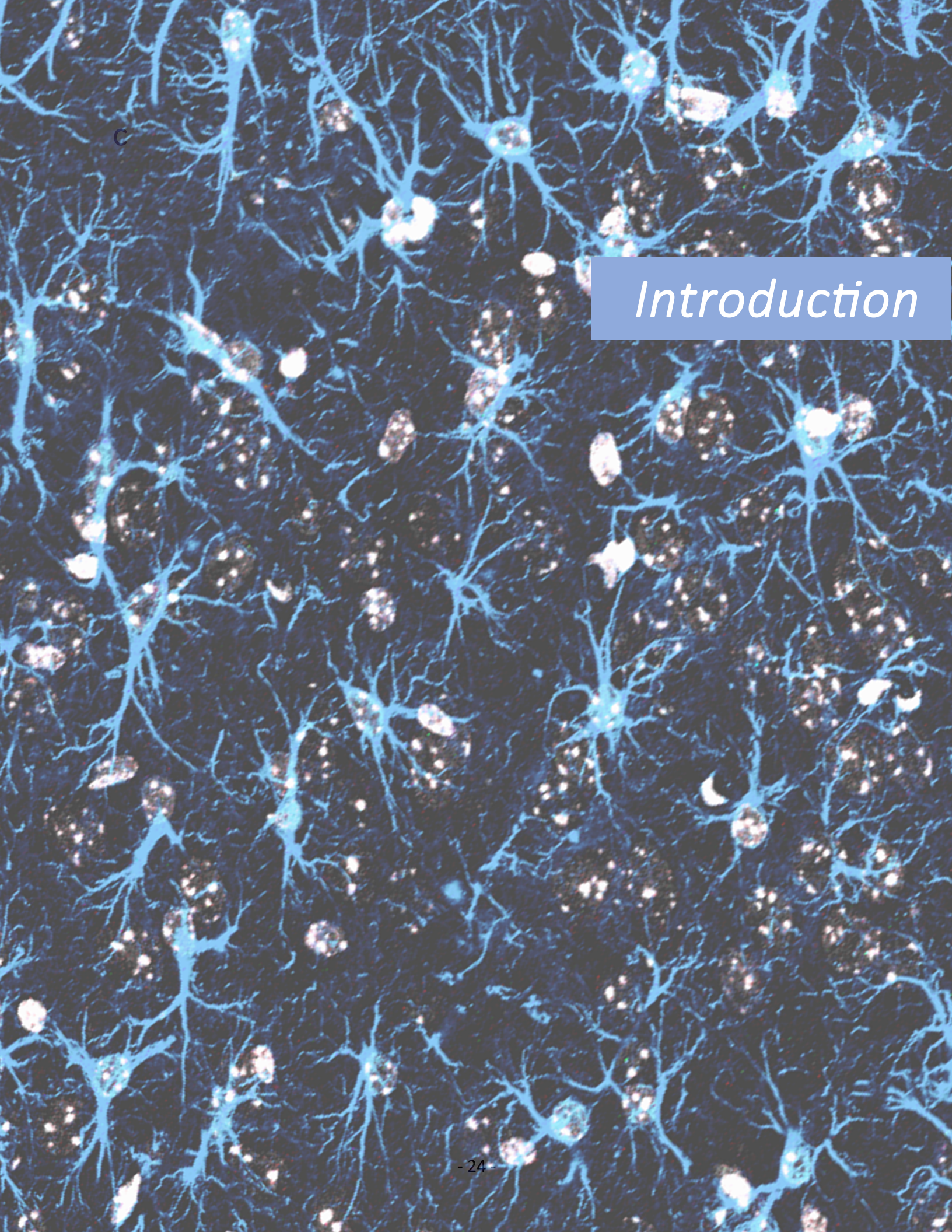

Introduction

Introduction

Glioblastoma overview

Gliomas are brain tumors originated by glial cells and represent around 70% of diagnosed malignant Central Nervous System (CNS) tumors. The most frequent type of glioma is glioblastoma (GBM), accounting for 50% of malignant CNS tumors (*1*). GBM is also the most aggressive type of CNS malignancy, and it is classified as a Grade 4 tumor, the highest degree of tumor malignancy according to the World Health Organization (WHO). Traditionally, CNS tumor grading and classification was based on histopathological tumor characteristics (*4*). However, more recent WHO guidelines for CNS tumor classification combine histopathological and molecular information in order to classify CNS tumors (*5*). According to the 2021 WHO guidelines, a glial tumor can be diagnosed as GBM if histopathological features like microvascular proliferation and necrosis are observed, in combination with an IDH-wildtype genetic background. Independently of histological characterization, genetic profiling of the samples can be performed and GBM diagnose can be confirmed if there is evidence of 1 or more of these 3 genetic alterations: TERT promoter mutation, EGFR amplification or copy number gain or loss of chromosomes 7 and 10, respectively (*6*).

Molecular profiling of GBM was also leveraged to classify tumors in order to try to stratify patients. The first classification by the TCGA divided GBM into classical, mesenchymal and proneural subtypes, defined by the alterations in EGFR, NF1 and PDGFRA, respectively (*7*). Later, the TCGA classification was integrated with single cell RNA-seq data from patients and experimental animal models, and this time GBM was classified according to their resemblance to the main cellular types in neural development. Thus, GBM can be astrocyte (AC)-like, oligodendrocyte progenitor cell (OPC)-like, neural progenitor cell (NPC)-like and mesenchymal (MES)-like. As in previous classifications, these subtypes were related to alterations in EGFR (AC-like), CDK4 (NPC-like), PDGFRA (OPC-like) and NF1 (MES-like) (*8*). However, GBM bears a high intra and inter-tumor heterogeneity, and studies found that multiple GBM subtypes could coexist in different tumor regions of the same patient (*9*). In fact, when different tumor regions from the same patient were laser-dissected and compared among patients, it was shown that samples from the same tumor region among patients were more similar to each other than different tumor regions from the same patient (*10*). To add another layer of complexity, GBM have also been classified according to their tumor microenvironment (TME) (*11*). Therefore, GBM heterogeneity hampers a tumor classification, the identification of GBM prognosis biomarkers, and the subsequent development of targeted therapies against the disease.

The current therapeutic standard of care to tackle GBM follows the Stupp method (*12*), which involves maximum safe tumor resection, followed by the application of radiation along with concurrent and adjuvant administration of temozolomide (TMZ) (*13, 14*). Recently, Tumor-Treating Fields (TTFields), antimitotic low-intensity electric fields, have been incorporated in

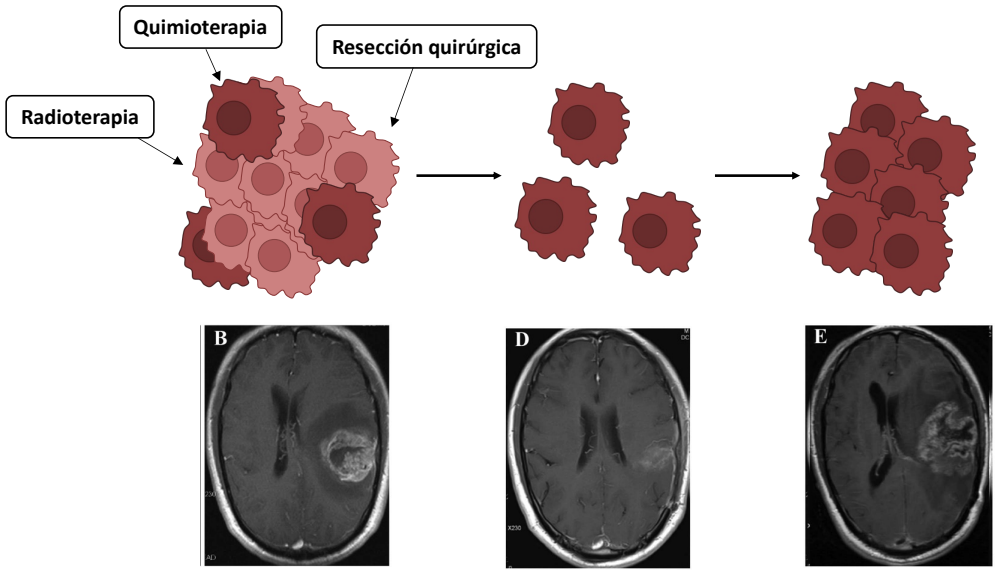

Scheme 1. GSC role in GBM recurrence. Modified from Zhou et al., 2016 (*2*)

combination with TMZ to the treatment options for patients, showing an enhancement in overall survival when compared to TMZ alone (*15, 16*). Unfortunately, despite the administration of current treatments, patients diagnosed with this devastating malignancy have a median survival of 20 months, and only around 5% of these patients survive for more than 5 years after being diagnosed (*17*).

Glioblastoma stem cells (GBM) and GBM cell of origin

One of the main reasons for therapeutic failure and poor prognosis in GBM is closely related to the cell composition of the tumors. As already mentioned, GBMs are highly heterogeneous tumors, and this heterogeneity handicaps an effective treatment of the disease. Part of underlying causes for such heterogeneity lies in a subpopulation of GBM cells known as glioblastoma stem cells (GSC) (*18*). GSCs have typical stem cell features as the ability to remain in a quiescent status, as well as self-renewal and multipotency capacities (*19, 20*). Each of these features confer GSCs a tool to promote GBM aggressiveness. The ability of GSCs to remain in a quiescent status, defined by a low proliferation rate, has been associated with treatment resistance (*21, 22*), as most chemotherapeutic drugs, including the gold standard TMZ and radiation, target cells with high DNA replication rates. Slow-proliferating GSCs have also shown high migration and invasive capacities (*23*) and, indeed, although most patient undergo surgical tumor debulking prior to the administration of chemotherapy or radiotherapy, the infiltrative nature of GBM hinders the complete elimination of infiltrative cells that are located deep into the brain parenchyma. This ability to escape current therapies combines with the fact that GSCs can self-renew and generate differentiated progeny, a GSC feature that allows them to regenerate tumors (Scheme 1)(*2*), creating new heterogeneous

populations of GBM cells (*24*). Altogether, the unique features of GSCs make them partly responsible for the malignancy of GBM and the frequent tumor recurrence in patients.

GSCs have been compared for a long time to their healthy neural stem cell (NSC) counterparts (*25*). This is due to their shared stem-cell features, described above, as well as the common biomarkers for their identification and classification such as Sox2 or Nestin (*24*). In fact, due to these similarities, several lines of evidence suggest that some GBMs originate from NSCs. Thus, mutations in NSCs from the subventricular zone (SVZ) in mice, but not in other glial cells or lineage committed neural cells, promote GBM development (*21, 26-28*). Confirming these studies, human GBM cells share critical mutations for GBM development with NSCs from the SVZ, suggesting that GBM cells arises from NSCs with driver mutations(*29*). Interestingly, among others, EGFR is one of the proteins whose alteration has been linked to the transition from NSCs to GSCs (*30*). On that note, NSCs with EGFR and/or other GBM driver-mutations are commonly studied as they provide important clues about GBM initiation, progression, and recurrence (*27, 28, 31, 32*).

Connexin43 and Src interplay in GBM

Connexins (Cxs) are transmembrane proteins formed by four transmembrane domains (M1-M4) with two extracellular (E1 and E2) loops and three intracellular regions: an intracellular loop (IL) and the N-terminal and C-terminal domains. Subunits of connexin organize as hexamers, generating the structure known as hemichannel or connexon, which can communicate the intracellular with the extracellular medium (*33*). Moreover, hemichannels among cells can interact forming GAP junctions, key channel structures for cell-cell communication (*34, 35*).

The most abundant connexin in mammals is connexin43 (Cx43). This connexin is highly expressed in heart and brain, where is mainly expressed in astrocytes, allowing them to perform key tasks for a healthy brain function (*36, 37*). Cx43 has widely studied channel-dependent and independent

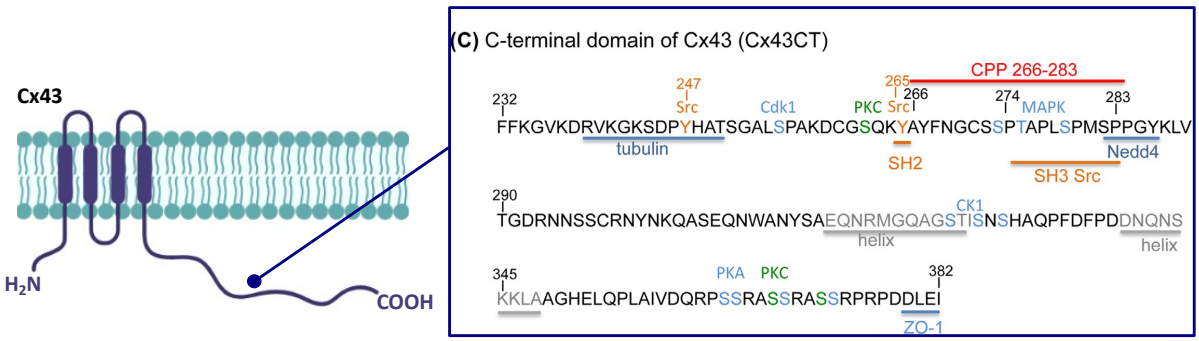

Scheme 2. Sequence and relevant regions of Cx43 C-terminus. Modified from Tabernero et al., 2016 (*3*)

functions (*38*). In this introduction, we will focus in the channel-independent functions of Cx43, and its fundamental task as a mediator of GBM cell signaling.

Cx43 has a complex role in the context of cancer, including GBM (*39*). An important evidence of an anti-tumorigenic role of Cx43 in the development of gliomas was a study that showed that transfection of glioma cells with Cx43 cDNA decreased their cell growth (*40*). Additionally, a study by Huang and colleagues, who described a correlation between levels of Cx43 and the malignancy and invasiveness features of gliomas. Thus, tumors with low expression of Cx43, such as GBM, exhibited more aggressive parameters (*41*). This tumor suppressor role of Cx43 in gliomas was confirmed with the decrease in tumor growth and stem cell potential that was observed after the ectopic administration of Cx43 in glioma cells (*42*). However, it should be noted that pro-tumorigenic functions of Cx43 have also been described in glioma models, such as the its involvement in mechanisms of TMZ resistance (*43*) and cell invasion (*44*). For a review of pro- and anti-tumor properties of Cx43 and other Cxs see (*39*). Therefore, the duality of Cx43 participation in tumor biology needs to be considered when developing new therapeutic approached based on this protein to tackle GBM.

Part of the pro- and anti-tumorigenic functions of Cx43 rely on its large C-terminal domain, which acts as a docking platform for the binding of multiple signaling effectors (Scheme 2) (*3, 39*). Among the most relevant proteins that bind Cx43 C-terminal domain is the proto-oncogene c-Src (*45*). c-Src is a non-receptor tyrosine kinase that belongs to the Src-family kinases (SFK) protein family, together with the ubiquitously expressed Fyn and Yes, and the rest of the family members that are normally expressed in hematopoietic cells (Lyn, Lck, Hck, Fgr, Blk and Yrk) (*46*). Src signaling functions involve the regulation of cell adhesion, migration, growth and survival processes (*47, 48*). The implication of Src in these signaling pathways that are normally upregulated in tumor progression, has placed Src in the spotlight of anti-tumor drug targets (*49-51*). Indeed, GBM tumors and, particularly, GSCs, exhibit a high Src activity (*52-54*). However, no SFK amplifications or mutations have been found in GBM patients, so the exacerbated activity of Src is considered a consequence of the activation of integrins and growth factor receptors, such as EGFR, commonly amplified or mutated in those patients (*55*). This high activation of Src and its related pathways has been implicated in GBM proliferation and invasiveness, angiogenic processes, autophagy, apoptosis, metabolism, and modulation of tumor microenvironment (*54-56*). Importantly, the upregulation of Src activity in GBM patients is associated with a poor median overall survival (*57*).

Src is tightly regulated by the phosphorylation of two residues within its SH1 kinase domain. Thus, the phosphorylation of tyrosine 527 (Y527) contributes to the maintenance of an inactive state, while the autophosphorylation of tyrosine 416 (Y416) enhances Src activity (*58*). This phosphorylation-dependent activity is therefore sensitive to the presence of additional kinases and phosphatases that participate in the regulation process. Indeed, the inhibition of Src requires the activity of the C-terminal c-Src kinase (CSK)(*59*), which phosphorylates Y527, and the additional role of phosphatases, such as the phosphatase and tensin homolog (PTEN), which removes

the phosphorylation of Y416 (*60*). Cx43, as previously mentioned, is able to recruit Src and its two activity modulators, ultimately inhibiting Src activity (*61-63*).

TAT-Cx43$_{266-283}$ as a GBM therapy

Leveraging the role of Cxs in cancer, several Cx-based strategies have been developed with therapeutic proposes against specific tumors (*64-67*). In our laboratory, a cell-penetrating peptide, which mimics the Src-inhibitory mechanism of Cx43 (TAT-Cx43$_{266-283}$), has been designed and studied deeply in GBM models. The structure of this peptide includes a TAT peptide, a sequence of physiologically positively-charged aminoacids that enables cellular internalization (*68*), fused to the sequence of residues 266-283 of Cx43, enclosed in the Src homology-3 (SH3) binding domain of Cx43 at its C-terminus tail (Scheme 2) (*3*). This small Cx43 fragment recapitulates the Src-inhibitory properties of Cx43, by acting as a docking platform for c-Src and its two endogenous inhibitors, CSK and PTEN, producing a downregulation of Src activity (Scheme 3) (*61, 69*). The Src-inhibitory properties of TAT-Cx43$_{266-283}$ have been used to target GSCs due to their previously mentioned high Src activity. Thus, when GSCs are treated with the cell-penetrating peptide, their proliferation is reduced and their stem cell phenotype is reversed (*63*). On that note, TAT-Cx43$_{266-283}$ is able to decrease GSC migration and invasiveness through the inhibition of the focal adhesion kinase (FAK) in freshly removed patient-derived GBM samples (*69*). Additionally, TAT-Cx43$_{266-283}$ administration in human GSCs inhibits their metabolic plasticity, decreasing their glucose uptake through an impairment of mitochondrial activities and a reduction in the expression of important metabolic targets in cancer, such as Glut-3 or hexokinase-2 (*70*). TAT-Cx43$_{266-283}$ has also shown to mediate human GSC cell death by a decrease in their autophagic flux upon treatment (*57*). Importantly, these results translate to in vivo models, in which the administration of TAT-Cx43$_{266-283}$ in a GBM mouse model with human GBM signatures (*71*) leads to an impaired tumor growth and ultimately, an increase in their survival (*72*). Altogether, the promising results obtained with the administration of the anti-tumor peptide TAT-Cx43$_{266-283}$ in GSCs represents an interesting and potential therapy to fight GBM.

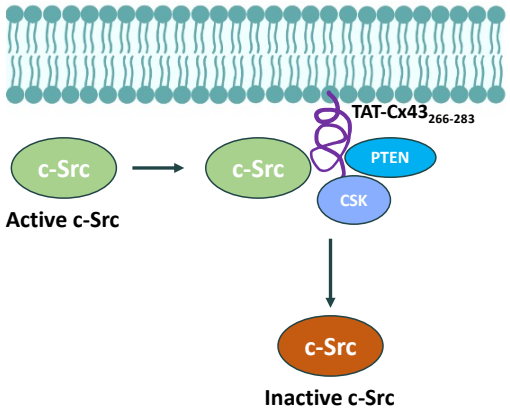

Scheme 3. Summary of the molecular mechanism of action of the anti-tumor peptide TAT-Cx43$_{266-283}$.

C

Objectives

Objectives

Glioblastoma is a devastating malignancy and there is an urgent need to develop new treatments to cure of the disease. The anti-tumor peptide TAT-Cx43$_{266-283}$, through the inhibition of c-Src, has shown promising results targeting GSCs in multiple preclinical GBM models. In this thesis, with the aim of boosting a future clinical application of TAT-Cx43$_{266-283}$, we investigated and covered some of the main gaps that hamper the translation of most preclinical results in clinical settings.

Therefore, the specific objectives of this thesis were:

1. To identify treatment response biomarkers of TAT-Cx43$_{266-283}$, in order to help with patient stratification and contribute to a more targeted and efficient application of the treatment.

2. To investigate the effect of TAT-Cx43$_{266-283}$ when it is administered within standard of care protocols, by combining its administration with the first-line tumor resection.

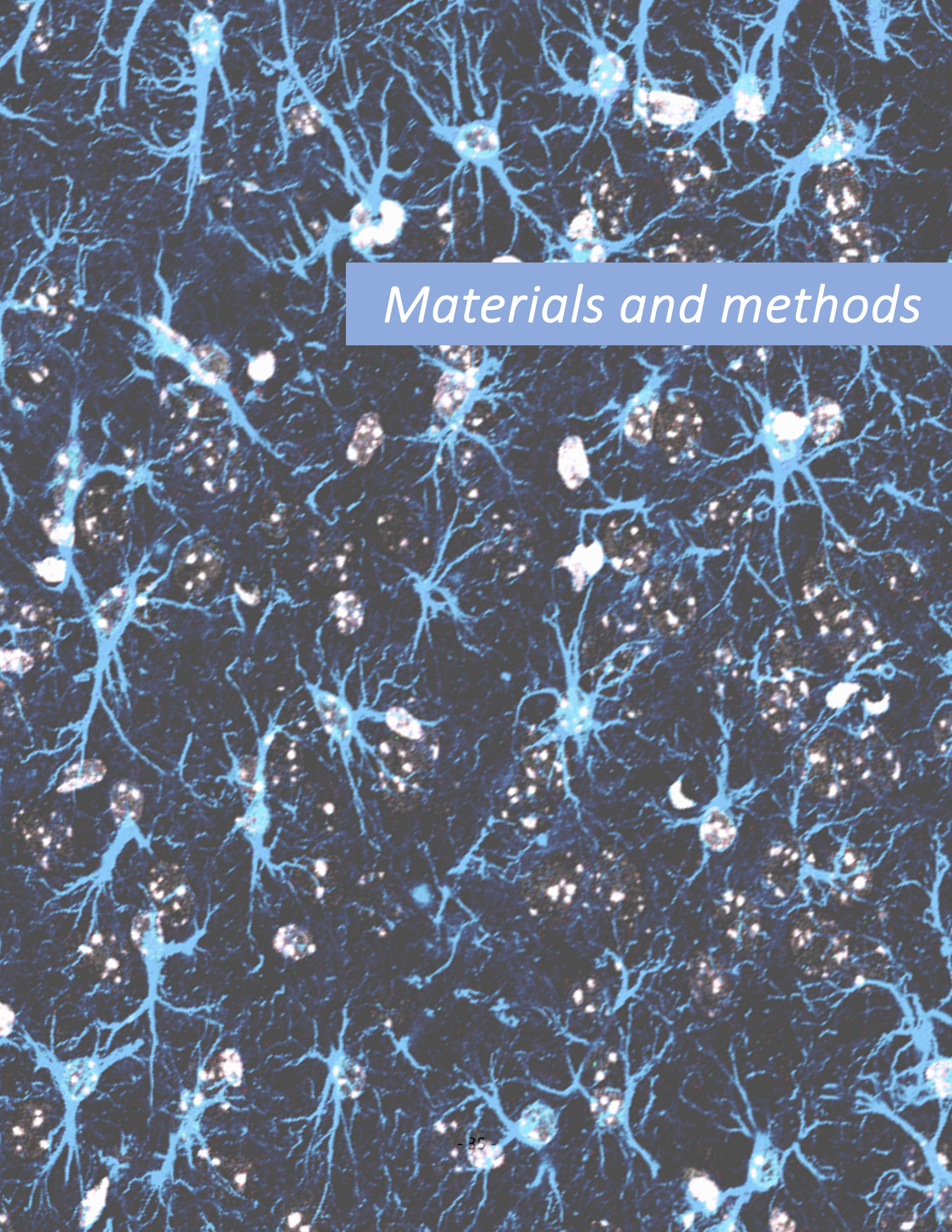

Materials and methods

Materials and methods

Animals

Equal number of male and female C57BL/6 mice were obtained from Charles River Laboratories, Jackson Laboratories and the animal facility of the University of Salamanca. Mice were housed in cages provided with environmental enrichment and food and water *ad libitum*, in a mouse room with a 12-hour light/12-hour dark light cycle. Animal procedures were approved by the ethics committee of the University of Salamanca and the Junta de Castilla y León (Spain) (CBE 697, 895 and 980) and were carried out in accordance with European Community Council directives (2010/63/UE), and Spanish law (RD 53/2013 BOE 34/11370–420, 2013) for the use and care of laboratory animals. Resection procedures were also performed in accordance with the protocols approved by the Institutional Animal Care and Use Committee (IACUC) at the Cleveland Clinic.

Cell culture

SVZ-NSCs, SVZ-EGFRwt and SVZ-EGFRvIII murine cell lines were generated by the Neuro-Oncology Unit (Instituto de Salud Carlos III, Madrid, Spain). These cell lines were obtained by retroviral expression of EGFRwt or EGFRvIII in primary SVZ NSCs from p16/p19 K.O. mice (*32*). These cell lines were cultured in DMEM/F-12 Glutamax medium (Gibco, ref: 31331028) supplemented with a mix of antibiotics and antimycotics [0.064 mg/mL penicillin G (Sigma, ref: P3032-10MU), 1 mg/mL streptomycin (Sigma, ref: S9137-25G) and 0.46 μg/mL amphotericin B (Sigma, ref: A9528-50MG)], as well as 1% B27 (Gibco, ref: 17504044), 0.5% N2 (Gibco, ref: 17502048), 20 ng/mL human EGF (Peprotech, ref: #AF-100-15) and 20 ng/mL human b-FGF (Invitrogen, ref: RP8628; Peprotech, ref: #100-18B).

Fetal human cortex NSCs were obtained from Takara Bio Inc. (ref.: Y40050). These cells were cultured in DMEM/F-12 Glutamax supplemented with the described mix of antibiotics and antimycotics, 10 ng/mL human EGF and 10 ng/mL human b-FGF. Cells were grown in adherent conditions adding 4 μg/mL laminin (R&D Systems, ref: 3446-005-01) to the medium.

NSC-EGFRvIII, NP, NPE and NPE-IE murine GSC lines, and the patient-derived GSC lines E15, E20, E22, E26, E28, E43 and E51 were obtained from the Glioma Cellular Genetics Resource (University of Edinburgh, Edinburgh, U.K.). NSC-EGFRvIII, NP, NPE and NPE-IE murine GSC lines were obtained by genetically modifying SVZ NSCs from C57BL/6 mice (*27*). NSCs-EGFRvIII are NSCs with EGFRvIII overexpression, NP are NSCs with CRISPR/Cas-mediated ablation of Nf1 and PTEN, NPE are NSCs with CRISPR/Cas-mediated ablation of Nf1 and PTEN and EGFRvIII overexpression, and NPE-IE are NSCs with CRISPR/Cas-mediated ablation of Nf1 and PTEN and EGFRvIII overexpression together with immune evasive properties developed after several intracranial transplantations in immunocompetent mice (*27*). NP, NPE and NPE-IE cell lines express GFP and luciferase as reporters. G166 human GSCs were obtained from Biorep and have been previously described (*73*). Patient-derived GSC lines L0, L1 and L2 were obtained from the University of Florida and have been previously described (*74*). T4121 cells were obtained from Duke University and have been described previously (*75*). DI318 cells were obtained from Cleveland Clinic and have been previously described (*76*). 23M cells were obtained from University of Texas/MD Anderson Cancer Center and have been previously described (*77*), and control immortalized hNSC were obtained from Fred Hutchinson Cancer Center/University of Washington and have been previously described (*78*). These cell lines were cultured in complete GSC medium: DMEM/F-12 with glutamine (Sigma, ref: D8437) supplemented with 1.45% glucose (Sigma, ref: G8644), 1% MEM Non-Essential Aminoacids 100X (Gibco, ref: 11140-035), 1% Penicillin-Streptomycin (Gibco, ref: 15140-122), 0.16% BSA (Gibco, ref: 15260-037), 0.2% β-mercaptoethanol (Gibco, ref: 31350-010), 1% B27, 0.5% N2, 10 ng/mL human EGF and 10 ng/mL human b-FGF. Either 4 μg/mL laminin (R&D Systems) or 0.06% Geltrex (Thermo Fisher, ref: A1413201) were added to the media, and TC-treated surfaces were used to ensure cell adherence. Additionally, E20, E26 and E51 lines were cultured in surfaces pre-coated with 10 μg/mL laminin (Invitrogen, ref: 23017-015) for at least 1 hour before use.

For quiescence experiments, NPE-IE cells were grown in growth factor-deprived medium supplemented with 40 ng/mL Bone Morphogenic Protein-4 (BMP-4) (R&D Systems, ref: 314-BPE-050).

GL261 GBM murine cell line was obtained from DSMZ. Cells were stably transfected with a pcDNA3.1-mCherry plasmid and the

subpopulation of mCherry GL261-GSC was isolated by Dr. Laura García-Vicente, as described (*79*). They were grown as spheres in complete GSC medium (described above).

SB28 GBM murine cell line was obtained from H. Okada (University of California, San Francisco). Cells were cultured in differentiation medium [(RPMI-1640 medium with L-glutamine (Sigma, ref: R8758) supplemented with 1% Penicillin-Streptomycin and 10% fetal bovine serum (FBS)] and grown in adherent conditions. The subpopulation of SB28-GSCs was isolated from SB28 cells as described (*79*) and cultured in adherent conditions in complete GSC medium (described above). 4 μg/mL laminin (R&D Systems) was added to the media, and TC-treated surfaces were used to ensure cell adherence.

Cells were grown until they were confluent, and Accutase (Corning, ref: 25-058-CI) was used for cell dissociation during passages. Cells were split according to the needs of the experiment and counted using a Countess Automatic Cell Counter (Invitrogen). All cell lines were cultured in an incubator with an atmosphere of 37°C and 5% CO_2. All cell lines were mycoplasma-free, and routinely tested for Mycoplasma spp. by PCR using a Mycoplasma Gel Form kit (Biotools, ref: 90.021-4542).

Treatments

Lyophilized peptides (>95% pure) were obtained from GenScript. YGRKKRRQRRR was used as the TAT sequence. TAT-$Cx43_{266–283}$ sequence was TAT-AYFNGCSSPTAPLSPMSP (patent ID: WO2014191608A1) (*80*) and TAT-$Cx43_{274-291}$ sequence was TAT-PTAPLSPMSPPGYKLVTG. TAT and TAT-$Cx43_{274-291}$ were used as control peptides, as they do not inhibit Src activity or exert antitumor effects (*57, 69, 81*).

For in vitro experiments, the peptides were dissolved in DMEM/F-12 medium and used at 50 μM in culture medium. Temozolomide (MedChemExpress, ref: HY-17364 or Sigma, ref: T2577-100MG) was dissolved in DMEM/F-12 medium and used at 100 μM in culture medium. Erlotinib (Sigma, ref: SML2156) was dissolved in filtered DMSO (Honeywell, ref: 41641) and DMEM-F12 medium, and used at 1 μM in culture medium. 0.05% (v/v) DMSO in DMEM-F12 medium was used as an erlotinib vehicle control. All treatments were added to the culture medium either once (24 hours after plating the cells) for protein extraction, or twice (24 and 96 hours after plating the cells) for cell viability experiments.

For in vivo experiments, an intracranial injection of 2 μL containing 200000 GSCs and 100 μM TAT-$Cx43_{266–283}$ in complete GSC medium, or the equivalent volume of complete GSC medium, was performed. One week after the injection of tumor cells, either 4 nmol/g TAT-$Cx43_{266–283}$ in 0.9% saline or the equivalent volume of 0.9% saline was intraperitoneally injected twice a week for the duration of the experiment as previously reported (*82*).

For the GL261-GSC model, an intracranial injection of 1 μL containing 5,000 GSCs and 100 μM TAT-$Cx43_{266–283}$ in 0.9% saline, or the equivalent volume of saline was performed. These animals did not receive intraperitoneal injections of the treatments.

For resection experiments, an injection of 20 μL of 0.9% saline or 100 μM TAT-$Cx43_{266-283}$ was performed in the intracranial cavity immediately after tumor resection or in the tumor area in sham operated mice. 3-5 days after tumor resection or sham operation, either 4 nmol/g TAT-$Cx43_{266–283}$ in 0.9% saline or the equivalent volume of 0.9% saline was intraperitoneally injected twice a week for the duration of the experiment.

Alamar blue viability assay

Either 1,000, 2,500 or 5,000 cells per well were plated in 96-well plates and treated as described. At the indicated times, cells were incubated with 10% Alamar blue/resazurin (Bio-Techne R&D Systems, ref: AR002, or Bio-Rad, ref: BUF01213) for 6 hours, and fluorescence was measured using an Appliskan microplate reader (λ_{ex} = 560 nm and λ_{em} = 590 nm).

MTT viability assay

5,000 cells per well were plated in 24-well plates and treated as described. At the indicated times, cells were incubated with 0.5 mg/mL MTT (Sigma, ref: M2128) for 75 minutes. Medium was removed and the MTT product was dissolved in DMSO and incubated for 10 minutes at room temperature and protected from direct light. Absorbance at 570 nm was measured using an Appliskan microplate reader.

Intracranial injection of GSCs

The murine GSC line NPE-IE was intracranially injected into the brains of 8-week-old C57BL/6 mice as previously described (*27*). Briefly, mice were anaesthetized with a mixture of 1.5-2% isoflurane and oxygen at a 1 L/min flow rate and placed in a stereotaxic frame. The skull

was trephined according to the stereotaxic coordinates, and 2 μL of complete GSC medium containing 200,000 cells were injected in the right striatum using a 26S-needle Hamilton microsyringe. Coordinates were +0.5 mm anterior-posterior (AP), +1.5 lateral-medial (LM) to bregma, and -2.5 mm deep. Before injecting at the described depth, a small pocket for the cells was formed by introducing the needle to a depth of -3.5 mm. The cell suspension was injected slowly, and the needle was held in place for 2 min after cell injection. Cells were kept on ice while the surgery was being performed. Animals received an intraperitoneal injection of 2 mg/kg meloxicam (Boehringer Ingelheim) and 0.1 mg/kg buprenorphine (Richter Pharma) for pain and inflammation management.

Animals were monitored daily during the first week after surgical procedures, and at least twice a week for the rest of the experimental period. Animals showing signs of humane endpoint (briefly, a decrease of 15-20% in their body weight, piloerection, hunched posture, lethargy or hyperexcitability) were sacrificed. An additional endpoint criterion was tumor size, indicated by luciferase activity of tumor cells.

For GL261-GSC model, the same surgical procedure was performed, but 1 μL of 0.9% saline containing 5,000 cells was injected in the right cortex. Coordinates were +1.5 mm AP, + 1,5 mm LM to lambda, and 2 mm deep.

GBM resection model

The murine GBM line SB28 grown in differentiation conditions was intracranially injected into the brains of 7-week-old C57BL/6 mice. Briefly, mice were anaesthetized with a mixture of 1.5-2% isoflurane and oxygen at a 2 L/min flow rate and placed in a stereotaxic frame. Then, 5 μL of RPMI medium containing 15,000 cells were injected in the right striatum using an insulin syringe. Coordinates were -1.5 mm AP, +1.5 LM to bregma, and -2 mm deep. Before injecting at the described depth, a small pocket for the cells was formed by introducing the needle to a depth of -2.5 mm. The cell suspension was injected slowly, and the needle was held in place for 30 seconds after cell injection. Cells were kept on ice while the surgery was being performed.

Ten days after tumor cell injection, when tumors had already developed, mice were subjected to resection or sham operation. All animals were anaesthetized with a mixture of 1.5-2% isoflurane and oxygen at a 2 L/min flow rate and places in a stereotaxic frame. The incision site was shaved and cleaned using 2% chlorhexidine + 70% isopropanol surgical

wipes (Iberomed, ref: BACTI010). Prior to the surgical procedure, animals were subcutaneously 4 mg/kg lidocaine (Richter Pharma) in the incision area. The incision was made using fine scissors (F.S.T.) and periosteum was removed using a sterile cotton swab. Then, the cell injection or tumor area was located, and a skull surgical window was opened using a surgical drill with a 2.7 mm diameter trephine (F.S.T.) in that area. For resection animals, the visible tumor was removed using a 2 mm curette (F.S.T.) and a vacuum aspirator coupled to an individual Pasteur pipette per animal. Once the tumor was removed and hemostasis was achieved, the cavity was filled with 20 μL of 0.9% saline or 100 μM TAT-$Cx43_{266-283}$. For sham animals, the tumor was not removed, and an intracerebral injection of 20 μL of 0.9% saline or 100 μM TAT-$Cx43_{266-283}$ was performed in the tumor area. Surgicel (Ethicon, ref: 1943) hemostat was used in sham and resected animals to help retain treatments, achieve hemostasis, and fill the surgical cavity in resected animals. The incision was closed using 5-0 Prolene suture (Ethicon, ref: EP8709H). Surgical instruments were sterilized between animals by immersion in 70% ethanol. Last, all animals were injected with 1 mL 0.9% saline and buprenorphine 0.1 mg/kg (Richter Pharma) to help with fluid recovery and analgesia, respectively. Ibuprofen 0.2 mg/mL (Kern Pharma) and neomycin 0.5 mg/mL (Gibco, ref: 21810031) were administered in the drinking water for 3 days post-operation. For that same period of recovery, mice were provided with Dietgel 76A (ClearH_2O) dietary supplement, additionally to their regular chow, to help with recovery.

Bioluminiscent in vivo imaging

Bioluminiscent imaging was performed approximately every two weeks after the implantation of the cells. Briefly, mice were intraperitoneally injected with 150 μg/g D-Luciferin (Goldbio, ref: LUCK-1G). Then, mice were anaesthetized with a mixture of 3% isoflurane and oxygen at a 1 L/min flow rate and, 10 minutes after the luciferin injection, they were imaged using an IVIS Lumina S5 (Perkin Elmer) for 5, 10, 30, 60 and 120 seconds of exposure. Binning parameters depended on the features (bioluminescence and size) of the tumor. For luciferase activity analysis, the software Living Image (Perkin Elmer) was used, and the same ROI was used for all the images. All exposure times were quantified, and the highest signal (measured in photons/s or p/s) was selected as the measure of luciferase activity for every mouse. This measure was used as an endpoint criterion if it was over 8.10^8 p/s, as it is an indicator of the tumor size.

Animals that did not show luciferase activity at day 27 after intracranial GSC injection, and signs of tumor presence (humane endpoint signs) were not included in the study. On that note, less than 50% injected mice developed tumors, despite following the protocol previously described (*27*).

Perfusion and tissue processing

When mice met the established humane endpoint criteria or the assigned experimental endpoint, they were intraperitoneally injected with 120 mg/kg sodium pentobarbital (Vetoquinol) and, upon loss of toe pinch reflex, they were transcardiacally perfused at a 5.5 mL/min flow rate. For immunofluorescence experiments, mice were perfused with 27.5 mL 0.9% NaCl and 55 mL 4% paraformaldehyde (PFA) (Panreac, ref: 252931) . Brains were extracted and kept in 4% PFA overnight, and then transferred to a cryoprotectant 30% sucrose in PBS solution until they sank. Then, brains were sliced to obtain 20 and 40 μm coronal sections using a Microm HM550 cryostat. 40 μm sections were maintained in a 1:1 PBS-glycerol solution at 20 °C until used. For histopathology experiments, mice were perfused with 27.5 mL 0.9% NaCl and 55 mL 4% PFA. Brains were extracted and kept in 4% PFA until used. Brains were sliced by the Compared Molecular Pathology service of Centre for Cancer Research (IBMCC, Salamanca) to obtain 3-5 μm coronal sections. For western blotting experiments, mice were perfused with 27.5 mL PBS (without antibiotics) and their brains were removed, snap-frozen using liquid nitrogen and kept at -80 °C until used. Brains were sliced to obtain 20 μm coronal sections using Microm HM550 cryostat.

Resection explant cultures

Immediately after brain extraction, approximately 1 mm^3 pieces were dissected from the tumors. Two explants per well were plated in 10 μg/mL laminin-coated 24-well plates in GSC medium (described in cell culture section). Explants were allowed to adhere to the culture surface for 72 hours, and either 100 μM TAT-$Cx43_{266–283}$ or the equivalent amount of DMEM/F-12 was added to the wells. Immediately after adding the treatments, cells were recorded using the time-lapse live cell imaging microscope Zeiss Axio Observer Z1, which acquired phase-contrast photographs of the cells every 10 minutes for 72-96 hours. Videos were processed using Zen imaging and Fiji softwares.

Immunofluorescence

For CD31 and GFP analyses, brain sections were washed with PBS with 0.1% Triton X-100

and blocked overnight with a blocking solution (PBS with 1% Triton X-100 and 10% donkey serum). Then, sections were incubated at 4°C overnight with a rat anti-CD31 monoclonal antibody (1:100, BD Biosciences, ref: 550274). Next, sections were washed with PBS with 0.1% Triton X-100 and incubated at 4°C overnight with a goat anti-rat IgG Alexa Fluor A594-conjugated secondary antibody (1:500, Invitrogen, ref: #A-11007). Finally, nuclei were stained with DAPI (1:5000, Invitrogen, ref: D3571) for 5 min and sections were mounted using SlowFade™ Gold antifade mountant (Thermo Fisher, ref: 536936). Mosaic images of the sections were acquired using a Leica Stellaris 8 confocal microscope, selecting only one plane of the z axis, and using a 10X objective. Images were processed and analyzed using the softwares LAS X (Leica) and Fiji.

For SVZ analyses, free-floating immunofluorescence was performed in 40 µm sections. Sections were washed with PBS and PBS-Tween 0.1%, and they were blocked for 45 r.t. with PBS-Tween 0.1% + NGS 1% + BSA 0.5%. Next, sections were incubated at 4 °C overnight with primary antibodies: rabbit anti-GFAP monoclonal antibody (1: 160, Sigma) and guinea pig anti-DCX monoclonal antibody (1:5000, Chemicon). Then, sections were washed with PBS-Tween 0.1% and incubated for 2 hours r.t. with the secondary antibodies: goat anti-rabbit IgG Alexa Fluor A594 and goat anti-guinea pig IgG Alexa Fluor A488 (1:500, Invitrogen). Finally, nuclei were stained with 1:5000 DAPI for 5 min and sections were mounted as described. Images were acquired using a Nikon Eclipse TE2000-S microscope coupled to a Leica DC 350F camera. Fluorescence intensity of the two SVZ of each section was analyzed with Fiji software.

Hematoxylin-eosin (H&E) staining

H&E staining was performed by the Compared Molecular Pathology service of Centre for Cancer Research (IBMCC, Salamanca). Bright-field images were acquired using an Olympus BX51 microscope coupled to an Olympus DP74 camera or with an Olympus Provis AX70 microscope coupled to an Olympus DP70 camera. Both microscopes were used with the software CellSens Entry 4.1.1.

Images from the resection experiments were evaluated with the help of the pathologist Dr. Carmen García Macías (University of Salamanca) and the neuropathologist Prof. Craig Horbinski (Northwestern University) Tumor necrosis and invasiveness were evaluated comparatively among tumor slices using a 0-5 score, and external proliferative foci were counted manually in each image.

Fluorescence In Situ Hybridization (FISH)

For FISH studies to analyze EGFR amplification in human GSC, 10^6 cells per GSC line were used. The Cytometry Service of the University of Salamanca performed FISH experiments using a EGFR/CEP7 probe (Metasystems).

RNA-seq

For RNA-seq analyses, 10^6 cells per cell line (L0, L1, L2, T4121, DI318, 23M and hNSC) were used. RNA was extracted by the DNA National Bank (University of Salamanca) using organic solvents (phenol-chloroform). The Sequencing Service (University of Salamanca) generated RNA libraries using a KAPA-mRNA HyperPrep-Kit for Illumina platforms (Roche). Sequencing was performed using a NovaSeq 6000 (Illumina).

EGFRvIII status was analyzed by aligning sequencing data to the human genome, and Sashimi plots were obtained using the software IGV (U.C. San Diego).

Lacunarity analyses

Blood vessel lacunarity was measured in at least four regions per animal from raw CD31 confocal mosaic images. Mean lacunarity and vessel area (i.e., CD31 area) were analyzed in these regions using the software AngioTool 0.6a (N.C.I., U.S.A.). Briefly, blood vessels were selected according to their intensity, non-specific small particles were removed and mean lacunarity was measured. Due to possible differences in mean lacunarity caused by a difference in the number of vessels in each region, values of vessel area and mean lacunarity were used to calculate a corrected lacunarity value (mean lacunarity x vessel area).

Western blots (WB)

WB were performed as previously described. Briefly, 100,000 cells were plated in 35 mm diameter dishes, and treated as described. 24 hours after the first dose of treatment, proteins were extracted using an extraction buffer (2% SDS, 2 mMM EDTA, 5 mM TRIS-HCl pH 6.8 and 2 mM EGTA in ddH_2O) with 1:100 protease (Fisher Scientific, ref: 12818395) and phosphatase inhibitor cocktails (Fisher Scientific, ref: 11833955). Samples were heated at 99°C for 5 min and sonicated for 5 min. Loading buffer 1X (Thermo Fisher, ref: NP0007) and reducing agent 1X (Thermo Fisher, ref: NP0004) were added to the samples and heated at 70°C for 10 min. Between 16-22 μg of proteins were loaded and separated on NuPaGE Novex Bis-Tris 4-12% midi gels (Invitrogen, ref: WG1402BOX) at room temperature and 120V. Proteins were

transferred to iBlot nitrocellulose membranes (Invitrogen, ref: IB23001) using an iBlot dry blotting system (Invitrogen). Ponceau staining (10%, Sigma, ref: P7170) was used to observe total protein load. Membranes were blocked with 5% dry milk and incubated overnight at 4°C with primary antibodies: anti-phospho-EGFR Y1068 (1:1000, Cell Signaling, ref: 3777) and anti-EGFR (1:1000, Cell Signaling, ref: 4267), anti-GAPDH (1:5000, Invitrogen, ref: AM4300) and anti-β-actin (1:1000, Sigma, ref: A5441). Then, membranes were washed and incubated with HRP-conjugated anti-rabbit IgG (1:2500, Santa Cruz Biotechnology, ref: sc-2357-CM) or HRP-conjugated anti-mouse IgG (1:5000, Jackson ImmunoResearch, ref: 115-035-003), and developed using luminol (Santa Cruz Biotechnology, ref: sc-2048) and a MicroChemi imaging system (Bioimaging Systems). Densitometry analysis of the protein bands was performed using Fiji software.

For frozen tumor tissue WB, three 20 μm coronal slices from frozen brains were cut. The tumor area was isolated and transferred to an Eppendorf containing 60 μL of protein extraction buffer with 1:100 protease and phosphatase inhibitor cocktails as described above. The processing of the samples was performed as described above. The primary antibodies used were: anti-phospho-Src Y416 (1:250, Cell Signaling, ref: 2101S) and anti-Src (1:500, Cell Signaling, ref: 2110S), and anti-β-actin (1:1000, Sigma, ref: A5441).

Patient protein levels, RNA expression and survival analysis

The Cancer Genome Atlas (TCGA) GBM database (*83*) (577 patients) was used for all the analyses, due to its patient number and reverse phase protein array (RPPA) data availability (193 patients). cBioportal (*84*)(https://www.cbioportal.org/) was used for downloading datasets and obtaining protein levels volcano plot and table. Thresholds for mRNA expression z-scores (relative to all samples) and protein level z-scores (RPPA)

were ± 2. RPPA data for p-Src Y416 levels and patient overall survival data were downloaded from cBioportal and plotted and analyzed using GraphPad Prism 9.0.1 P-Src Y416 and *EGFR* correlation graph was obtained from GlioVis portal (*85*)(http://gliovis.bioinfo.cnio.es/).

Statistical analysis

Results are expressed as the means ± S.E.M of at least 3 independent experiments. For comparisons between two groups, data were analyzed by two-tailed Student's t-test. For

comparisons between more than two groups, data were analyzed by one- and two-way ANOVA, followed by a post-hoc Tukey test. For survival analyses, data were represented in a Kaplan-Meier curve and differences were compared using a Log-rank test. Differences between groups were considered significant when p value < 0.05.

Chapter 2: Discussion

Our previous studies in different preclinical models suggest that the antitumor peptide TAT-Cx43$_{266-283}$ is a promising therapy against GBM, as it reduces GSC proliferation and invasiveness and modifies their metabolism, ultimately extending the survival of GBM-bearing mice (*69, 70, 72*). In the present study, we provide further evidence that supports the potential clinical benefits of this peptide in combination with GBM resection.

The SB28 GBM mouse model is a recent preclinical model that is interesting for the field due to its poor immunogenic potential, which resembles GBM immunosuppressive nature, making it a good model for immunotherapy studies (*131, 132*). However, a downside of this model is that it has barely been described in articles, so further characterization is needed (*133*). In this study, we contributed to the histological characterization of this model by showing that SB28 tumors indeed recapitulate important histological features of human GBM: pseudopalisading necrosis (*126*), infiltrative borders with proliferative external foci (*127*) and the presence of spindle-shaped cells (*130*).

As tumor resection is the first-line treatment against GBM, we performed tumor resection surgery in the SB28 GBM mouse model. We observed that, although not significantly, tumor resection seemed to prolong the survival of tumor-bearing mice. However, in line with previous studies (*122, 123*), we found that tumor resection increased the aggressiveness of the remaining tumor cells, as shown by the increase in infiltrative borders and external proliferative foci that we observed in tumor resected mice when compared to sham mice. Importantly, the combination of tumor resection with TAT-Cx43$_{266-283}$ administration significantly enhanced the survival of SB28-bearing mice, and strongly reduced the GBM histological hallmarks of invasiveness.

Gaining insight into the mechanism underlying these effects, we found that resected mice showed increased levels of Src activity in regrown tumors when compared to sham mice. Src is a target of TAT-Cx43$_{266-}$

$_{283}$ (*63*), which explains the improved outcomes of TAT-Cx43$_{266-283}$ administration in resected mice, whose tumors had higher activity of Src than sham mice. Indeed, resected mice had a better prognosis after TAT-Cx43$_{266-283}$ treatment, as shown by the enhanced survival and significant decrease in the invasive features of the model after treatment. On that note, Src is a key player in migration and invasion, which is in agreement with the increased invasiveness observed after tumor resection that is impaired by TAT-Cx43$_{266-283}$ (*52, 69, 134, 135*). In addition, Src is related to the maintenance of stemness in GSCs (*72, 93, 136*), so the increase in Src levels observed after resection is in line with previous findings about the increased number of GSC and stem cell features of the tumor after resection (*123*). Our in vitro studies showed that TAT-Cx43$_{266-283}$ decreased SB28-GSC viability but had no effects on SB28 cultured in differentiation conditions. Altogether, these and the in vivo results seem to indicate that TAT-Cx43$_{266-283}$ effectively targets the infiltrative GSC population that remains after tumor resection, which is consistent with the beneficial effects of TAT-Cx43 in GBM resected mice.

One of the challenges of treating GBM and the rest of brain tumors are the physiological barriers between the brain and the rest of the system. The blood-brain barrier (BBB) is the main barrier between the systemic blood and the brain, and due to a tightly regulated transportation of molecules between these two compartments, it hinders the entry of most drugs into the brain and therefore, into the tumor area (*137*). Large tumors can disrupt this barrier and enhance its permeability, transforming it into what is known as blood-brain-tumor barrier (BBTB). However, the heterogeneity of brain tumors, as well as the presence of tumor cells far from the BBB-disruptive tumor mass, hampers this permeability enhancement in all tumor areas and makes the BBTB, together with the BBB, an obstacle to overcome when administering systemic treatments (*138*). Hence, the post-surgical tumor intracavity administration is an interesting strategy to overcome the physiological barriers. In fact, one of the ways of administering chemotherapy is the insertion of chemotherapy wafers in the resected tumor area during surgery (*139, 140*) and some studies have used this intracavitary approach for emerging

therapies against GSCs (*141*). Importantly, the present study shows the safety and efficiency of TAT-Cx43$_{266-283}$ administration in the intracranial cavity post-tumor resection in GBM-bearing mice.

Although further research is required to optimize dose and administration schedule parameters, as well as to improve the form in which TAT-Cx43$_{266-283}$ is administered to ensure an optimal beneficial effect of the treatment, the positive results of TAT-Cx43$_{266-283}$ treatment in combination with tumor resection supports its progression towards a clinical trial.

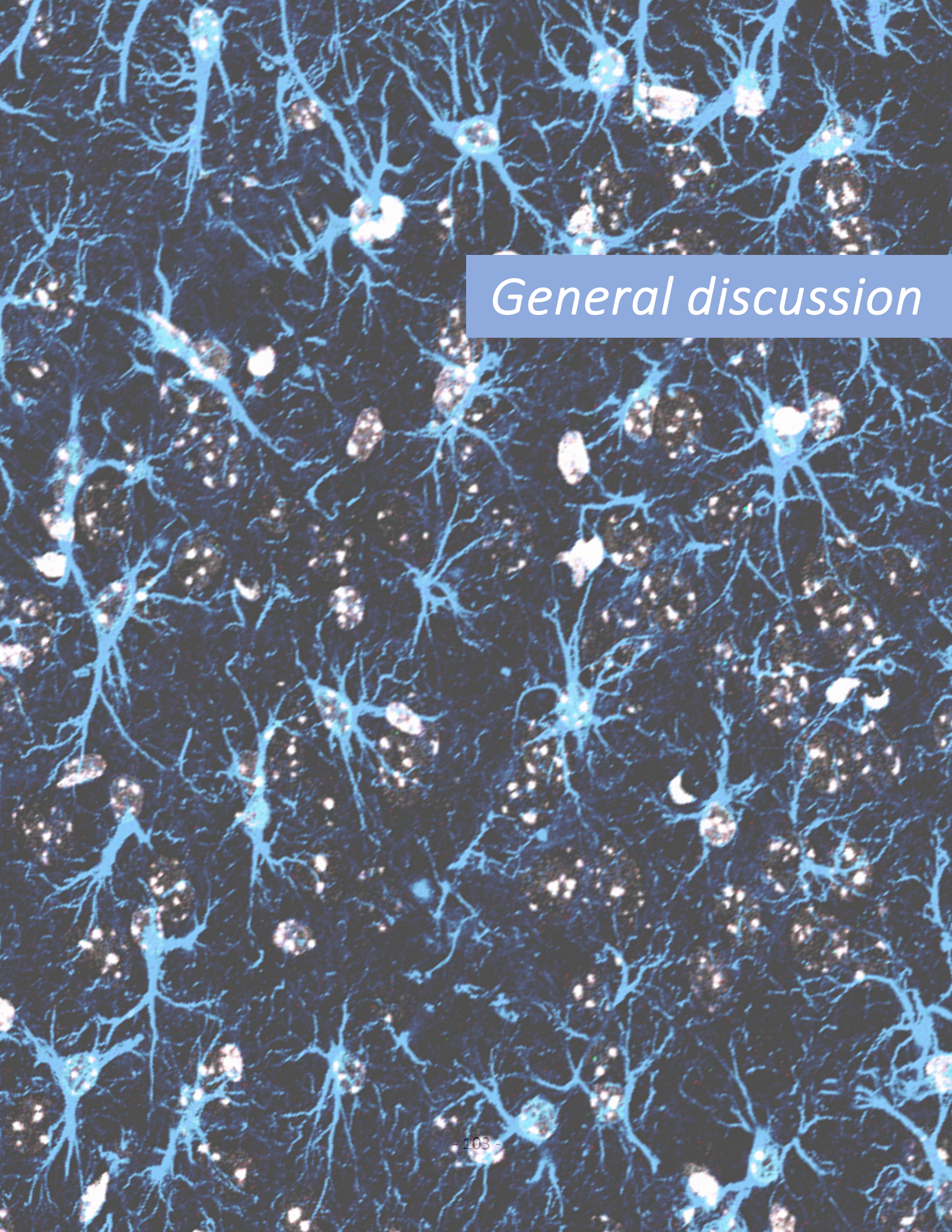

General discussion

General discussion

Glioblastoma is one of the deadliest malignant tumors worldwide and it remains incurable. Despite unceasing effort to tackle the disease from basic, translational, and clinical perspectives, current therapies fail to prolong patient survival for more than 14-20 months after tumor diagnose (*16*). The underlying reason for this therapeutic failure involves some of the unique features of GBM that allow it to evade current treatments and ultimately generate tumor recurrence. One of the main difficulties to be faced are the high intratumor and interpatient heterogeneity in GBMs (*11, 142*), which hamper the development of a standard treatment for all GBM patients and make it difficult to predict the outcome of current treatments. On that note, there is an urgent need for identifying treatment response biomarkers for cell subpopulations and GBM subtypes that enable a better patient stratification and therefore a more efficient treatment system for GBM patients (*143*). Moreover, even when drugs seem to be successful in preclinical GBM models, most of them fail when administered in clinical trials, partly due to the particular location of GBM in the organism. The blood-brain barrier (BBB) strictly regulates and allows the entrance of molecules from the systemic blood to the brain, and most GBM drugs are not able to overcome this barrier, leading to poor outcomes in clinical settings (*137, 138, 144*), and impels the development of drug administration methods that overcome the BBB (*145*). Additionally, drugs in the clinic are often administered after tumor resection (*13, 14*) which, despite increasing patient survival in most of the cases (*117*), has been associated to a reshape of the remaining GBM cells, increasing their aggressiveness (*122, 146-148*). On that note, current preclinical models unsuccessfully attempt to mimic GBM heterogeneity due to the difficulty of combining the genetic features of patient-derived lines with the tumor microenvironment of orthotopic xenografts. These models also fail to replicate a clinical administration protocol as most of them focus on treating intact intracranial tumors instead of performing the previous surgical resection included in the standard of care (*149*), thus hindering the translation of preclinical results to a clinical setting.

We developed a Src-inhibitory peptide that has shown antitumor properties in preclinical GBM models, decreasing the proliferation and invasiveness of GSCs, inhibiting their metabolic plasticity (*70*) and increasing the survival time of GBM bearing mice (*69, 72*). In this thesis, we have aimed to address some of the main points that hamper a successful translation from preclinical to clinical results.

Although, as mentioned, GBMs are heterogeneous, we have identified a subset of patients that might experience a higher benefit from TAT-$Cx43_{266-283}$ treatment. Our results in murine and patient-derived GBM cells have shown that EGFR alterations (EGFR amplification and EGFRvIII mutation) in these tumors predict and participate in their response of TAT-$Cx43_{266-283}$, which implies that TAT-$Cx43_{266-283}$ can be considered a targeted therapy. Importantly, around 50% of GBM patients have alterations in EGFR (*87*), so these preclinical results suggest that the administration of TAT-$Cx43_{266-283}$ as a GBM therapy might be effective in at least half of GBM patients. On that note, the positive results obtained in the variety of preclinical in vitro and in vivo models that have undergone TAT-$Cx43_{266-283}$ treatment in this thesis (NPE-IE and SB28 GBM models) and previous works from our group (G166, GL261 and GL261-GSC GBM models (*72*)) in addition to the positive effects in freshly removed samples from different GBM patients (*69*) show that TAT-$Cx43_{266-283}$ is effective in a great variety of GBM models, originated from different cells, some of them proposed to resemble the most frequent human GBM subtype (*71*), representing the high intertumor heterogeneity of the clinic of GBM.

Moreover, the fact that EGFR alterations act as a predictor of treatment response may allow the selection and stratification of patients in a clinical trial. Importantly, GBM patient samples are routinely tested for EGFR alterations, as EGFR amplification is a diagnose biomarker of GBM (*6*). The general availability of EGFR status data would not make it necessary to test patients prior to being enrolled on a clinical trial, saving time and resources, and therefore allowing a more efficient and straight-forward experimental design of the trial with better options to achieve benefits for the selected patients.

As mentioned before, tumor resection is the first-line treatment for most patients, and the base for the administration of adjuvant therapies. Tumor resection has been found to reshape GBM and its microenvironment (*122, 150*), turning tumors into more aggressive

phenotypes and increasing the GSC population in the tumor (*123*), a GBM subpopulation responsible for GBM recurrence. Indeed, we found that tumor resection increased GBM infiltration and the combination of tumor resection with TAT-$Cx43_{266-283}$ was able to decrease invasive features of the tumors and ultimately achieve better survival outcomes. These are promising results, however, the current standard of care for GBM also involves the administration of TMZ and radiotherapy (*13*), administered after tumor resection. Therefore, it would be interesting to study whether the administration of TMZ and radiotherapy after tumor resection would constitute an optimized therapeutic scenario for the adjuvant administration of TAT-$Cx43_{266-283}$.

On that note, in order to bypass the BBB and leverage the unique administration route generated by tumor resection, in this thesis we administered TAT-$Cx43_{266-283}$ in the tumor cavity. This administration route allowed the injection of larger treatment volumes and a direct contact of the treatment with tumor border area, an area of interest due to the presence of infiltrative GBM cells that are often responsible for tumor recurrence (*151*). Our results show that intracavitary administration of TAT-$Cx43_{266-283}$ has not only shown to be effective reducing tumor invasiveness and aggressiveness, but it has also shown to be a safe administration route in murine models. Consistent with this, the results in this thesis allow to confirm the cell selectivity of TAT-$Cx43_{266-283}$ as it targets GSCs but it does not affect cell viability of human and murine NSC cell lines, despite the described similarities between the two cell types (*25*).

Importantly, our results have also showed that TAT-$Cx43_{266-283}$ is more effective than TMZ and erlotinib in vitro, and that the combination of TAT-$Cx43_{266-283}$ and erlotinib administration in some murine GSCs has a synergistic effect. These results, together with the analysis from GBM patient data sets, reinforce the importance of targeting EGFR-Src axis in GBMs. Indeed, our results confirm the inclusion of EGFR, in addition to Src, to the targets of TAT-$Cx43_{266-283}$. Interestingly, a combined targeting of Src and EGFR in GBMs has already demonstrated to be beneficial for the reversal of treatment resistance with an ultimate enhancement of survival in murine preclinical GBM models (*102*).

Although further research is required to optimize dose schedules and administration routes, as well as to determine pharmacokinetic and pharmacodynamic

parameters, our results conclude that TAT-$Cx43_{266-283}$ is a targeted therapy against the EGFR-Src axis, which might be beneficial for a high percentage of GBM patients, especially after tumor resection.

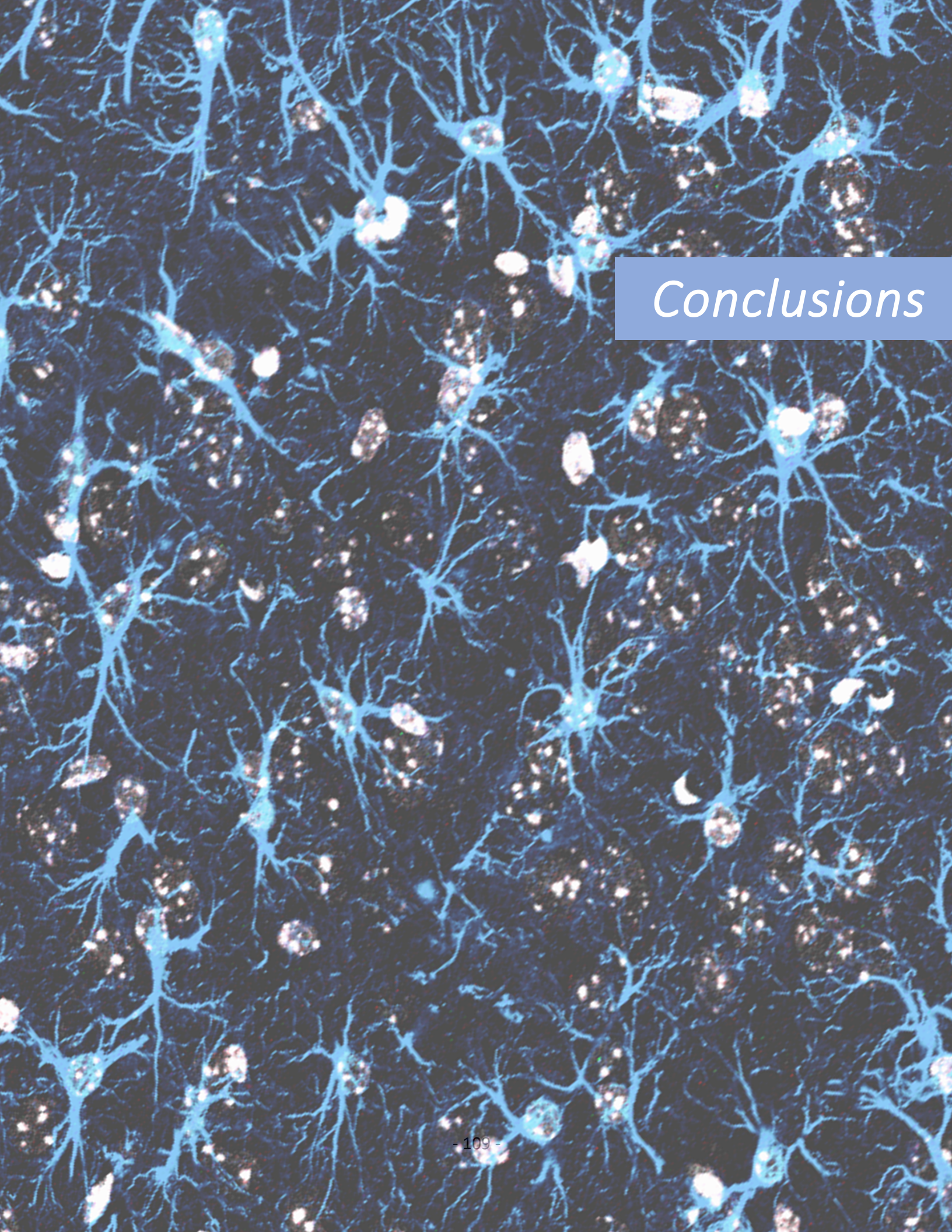

Conclusions

Conclusions

I. The frequent EGFR alterations (EGFR amplification and EGFRvIII) predict the response to TAT-$Cx43_{266-283}$ treatment in murine and patient-derived GSCs, which may help with patient stratification in future clinical trials and treatments.

II. EGFR alterations participate in the response to TAT-$Cx43_{266-283,}$ as judged by different in vitro and in vivo GBM models generated by neural stem cells with EGFR alterations.

III. TAT-$Cx43_{266-283}$ specifically targets EGFR altered neural and glioblastoma stem cells, sparing healthy murine and human neural stem cells.

IV. EGFR alterations correlate with higher levels of Src activity (p-Y416), and with shorter patient overall median survival.

V. Treatment with TAT-$Cx43_{266-283}$ in GSCs is more effective than the standard of care chemotherapeutic temozolomide and the classical EGFR inhibitor erlotinib. Interestingly, the combination of erlotinib and TAT-$Cx43_{266-283}$ had a synergistic effect in some murine GSCs.

VI. Tumors of SB28 GBM mouse model recapitulate histopathological features of human GBMs, like pseudopalisading necrosis, infiltrative borders, proliferative spread foci and spindle-shaped cells.

VII. Tumor resection in the SB28 GBM model increased, although not significantly, survival time compared to sham group. Tumors grown after resection exhibited an increase in aggressive features and Src activity when compared to their sham counterparts.

VIII. TAT-$Cx43_{266-283}$ administration in the resection cavity has shown antitumor efficacy as well as safety in in the SB28 GBM model.

IX. The combination of tumor resection and TAT-$Cx43_{266-283}$ intracavitary administration reduced the invasive features observed after resection, and ultimately increased survival time in the SB28 GBM model, which support the administration of TAT-$Cx43_{266-283}$ following the standard of care in the clinic, in which tumor resection is the first-line treatment.

Final conclusion

Results obtained in this PhD thesis constitute a crucial progress in the translation of TAT-Cx43$_{266-283}$ antitumor peptide for the treatment of GBM. Indeed, we have identified a substantial subgroup of GBM patients that may benefit from this treatment, and we have found a positive effect of administering TAT-Cx43$_{266-283}$ upon tumor resection, a scenario that resembles closely to the current clinical setting. Altogether, these results serve as a base for future clinical investigations and, together with previous studies, support the therapeutic potential of TAT-Cx43$_{266-283}$ as a treatment for GBM.

Conclusión final

Los resultados obtenidos en esta tesis doctoral suponen un avance en la traslación del péptido antitumoral TAT-Cx43 para el tratamiento del GBM. Hemos identificado un subgrupo numeroso de pacientes de GBM que podrían beneficiarse del tratamiento en futuros ensayos clínicos, y a además hemos encontrado un efecto positivo de la administración de TAT-Cx43$_{266-283}$ tras la resección del tumor, un escenario que se acerca a la situación clínica actual. En conjunto, estos resultados sirven como base para futuras investigaciones clínicas y, junto con estudios previos, apoyan el potencial terapéutico de TAT-Cx43$_{266-283}$ como tratamiento del GBM.

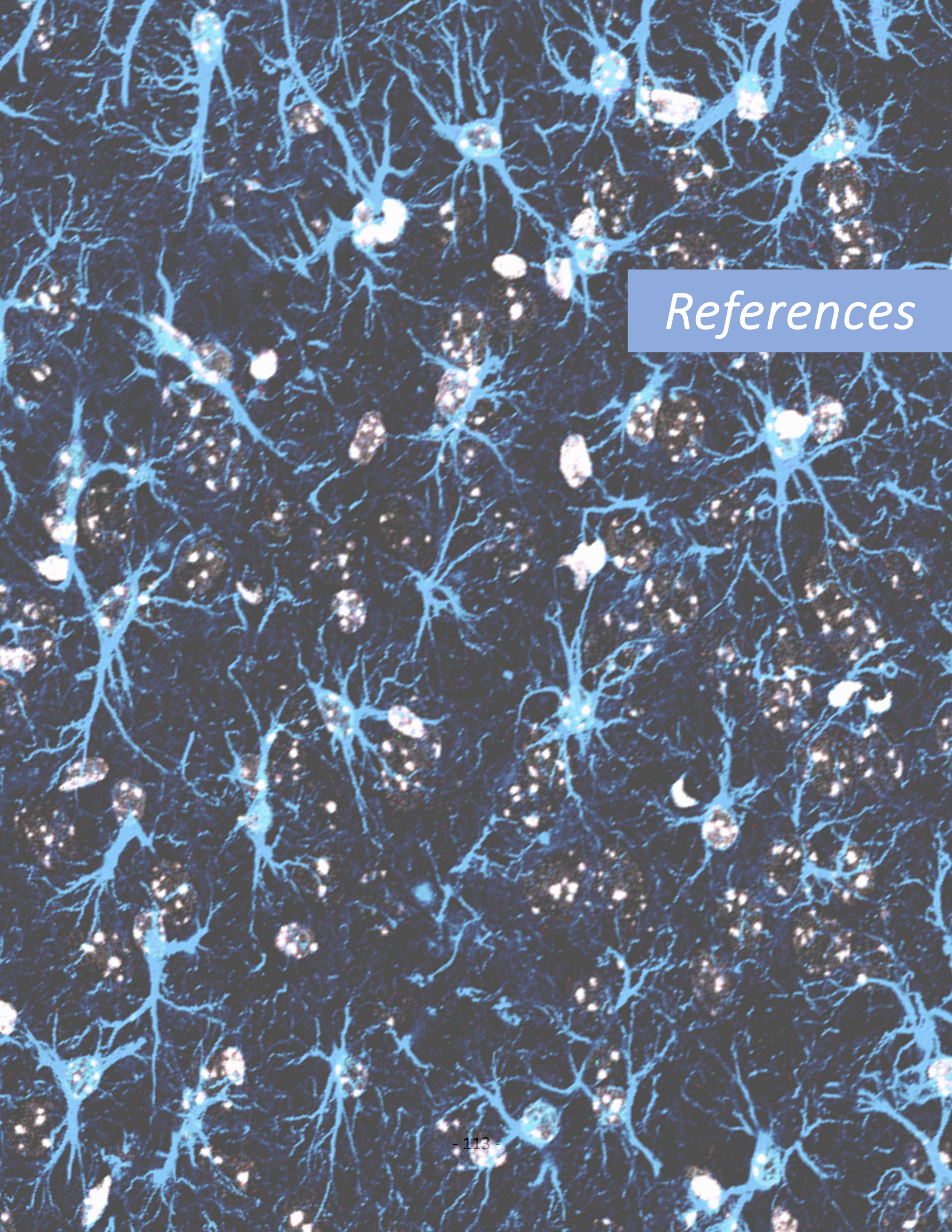

References

References

1. K. D. Miller *et al.*, Brain and other central nervous system tumor statistics, 2021. *CA Cancer J Clin* **71**, 381-406 (2021).

2. X. Zhou *et al.*, Recurrence patterns in patients with high-grade glioma following temozolomide-based chemoradiotherapy. *Mol Clin Oncol* **5**, 289-294 (2016).

3. A. Tabernero, E. Gangoso, M. Jaraíz-Rodríguez, J. M. Medina, The role of connexin43-Src interaction in astrocytomas: A molecular puzzle. *Neuroscience* **323**, 183-194 (2016).

4. D. N. Louis *et al.*, The 2007 WHO classification of tumours of the central nervous system. *Acta Neuropathol* **114**, 97-109 (2007).

5. D. N. Louis *et al.*, The 2016 World Health Organization Classification of Tumors of the Central Nervous System: a summary. *Acta Neuropathol* **131**, 803-820 (2016).

6. D. N. Louis *et al.*, The 2021 WHO Classification of Tumors of the Central Nervous System: a summary. *Neuro Oncol* **23**, 1231-1251 (2021).

7. R. G. Verhaak *et al.*, Integrated genomic analysis identifies clinically relevant subtypes of glioblastoma characterized by abnormalities in PDGFRA, IDH1, EGFR, and NF1. *Cancer Cell* **17**, 98-110 (2010).

8. C. Neftel *et al.*, An Integrative Model of Cellular States, Plasticity, and Genetics for Glioblastoma. *Cell* **178**, 835-849.e821 (2019).

9. A. P. Patel *et al.*, Single-cell RNA-seq highlights intratumoral heterogeneity in primary glioblastoma. *Science* **344**, 1396-1401 (2014).

10. R. B. Puchalski *et al.*, An anatomic transcriptional atlas of human glioblastoma. *Science* **360**, 660-663 (2018).

11. K. White *et al.*, Identification, validation and biological characterisation of novel glioblastoma tumour microenvironment subtypes: implications for precision immunotherapy. *Ann Oncol* **34**, 300-314 (2023).

12. R. Stupp *et al.*, Radiotherapy plus concomitant and adjuvant temozolomide for glioblastoma. *N Engl J Med* **352**, 987-996 (2005).

13. R. Kotecha, Y. Odia, A. A. Khosla, M. S. Ahluwalia, Key Clinical Principles in the Management of Glioblastoma. *JCO Oncol Pract* **19**, 180-189 (2023).

14. N. C. C. Network. PDF link: https://www.nccn.org/professionals/physician_gls/pdf/cns.pdf

15. B. Fekete *et al.*, What predicts survival in glioblastoma? A population-based study of changes in clinical management and outcome. *Front Surg* **10**, 1249366 (2023).

16. R. Stupp *et al.*, Effect of Tumor-Treating Fields Plus Maintenance Temozolomide vs Maintenance Temozolomide Alone on Survival in Patients With Glioblastoma: A Randomized Clinical Trial. *JAMA* **318**, 2306-2316 (2017).

17. M. T. C. Poon, C. L. M. Sudlow, J. D. Figueroa, P. M. Brennan, Longer-term (≥ 2 years) survival in patients with glioblastoma in population-based studies pre- and post-2005: a systematic review and meta-analysis. *Sci Rep* **10**, 11622 (2020).

18. A. Lauko, A. Lo, M. S. Ahluwalia, J. D. Lathia, Cancer cell heterogeneity & plasticity in glioblastoma and brain tumors. *Semin Cancer Biol* **82**, 162-175 (2022).

19. K. Mohammad, P. Dakik, Y. Medkour, D. Mitrofanova, V. I. Titorenko, Quiescence Entry, Maintenance, and Exit in Adult Stem Cells. *Int J Mol Sci* **20**, (2019).

20. D. Bhartiya, K. R. Boheler, P. Rameshwar, Multipotent to pluripotent properties of adult stem cells. *Stem Cells Int* **2013**, 813780 (2013).

21. J. Chen *et al.*, A restricted cell population propagates glioblastoma growth after chemotherapy. *Nature* **488**, 522-526 (2012).

22. X. P. Xie *et al.*, Quiescent human glioblastoma cancer stem cells drive tumor initiation, expansion, and recurrence following chemotherapy. *Dev Cell* **57**, 32-46.e38 (2022).

23. R. J. Atkins *et al.*, Cell quiescence correlates with enhanced glioblastoma cell invasion and cytotoxic resistance. *Exp Cell Res* **374**, 353-364 (2019).

24. J. D. Lathia, S. C. Mack, E. E. Mulkearns-Hubert, C. L. Valentim, J. N. Rich, Cancer stem cells in glioblastoma. *Genes Dev* **29**, 1203-1217 (2015).

25. A. Lombard *et al.*, The Subventricular Zone, a Hideout for Adult and Pediatric High-Grade Glioma Stem Cells. *Front Oncol* **10**, 614930 (2020).

26. S. Alcantara Llaguno *et al.*, Malignant astrocytomas originate from neural stem/progenitor cells in a somatic tumor suppressor mouse model. *Cancer Cell* **15**, 45-56 (2009).

27. E. Gangoso *et al.*, Glioblastomas acquire myeloid-affiliated transcriptional programs via epigenetic immunoediting to elicit immune evasion. *Cell* **184**, 2454-2470.e2426 (2021).

28. S. Alcantara Llaguno *et al.*, Cell-of-origin susceptibility to glioblastoma formation declines with neural lineage restriction. *Nat Neurosci* **22**, 545-555 (2019).

29. J. H. Lee *et al.*, Human glioblastoma arises from subventricular zone cells with low-level driver mutations. *Nature* **560**, 243-247 (2018).
30. A. Ayuso-Sacido *et al.*, Activated EGFR signaling increases proliferation, survival, and migration and blocks neuronal differentiation in post-natal neural stem cells. *J Neurooncol* **97**, 323-337 (2010).
31. X. Wang *et al.*, Sequential fate-switches in stem-like cells drive the tumorigenic trajectory from human neural stem cells to malignant glioma. *Cell Res* **31**, 684-702 (2021).
32. R. Gargini *et al.*, The IDH-TAU-EGFR triad defines the neovascular landscape of diffuse gliomas. *Sci Transl Med* **12**, (2020).
33. R. Talaverón *et al.*, Neural progenitor cells isolated from the subventricular zone present hemichannel activity and form functional gap junctions with glial cells. *Front Cell Neurosci* **9**, 411 (2015).
34. N. Genet, N. Bhatt, A. Bourdieu, K. K. Hirschi, Multifaceted Roles of Connexin 43 in Stem Cell Niches. *Curr Stem Cell Rep* **4**, 1-12 (2018).
35. C. Giaume, C. C. Naus, J. C. Sáez, L. Leybaert, Glial Connexins and Pannexins in the Healthy and Diseased Brain. *Physiol Rev* **101**, 93-145 (2021).
36. C. Giaume, C. C. Naus, Connexins, gap junctions, and glia. *Wiley Interdisciplinary Reviews: Membrane Transport and Signaling* **2**, 133-142 (2013).
37. C. Giaume *et al.*, Gap junctions in cultured astrocytes: single-channel currents and characterization of channel-forming protein. *Neuron* **6**, 133-143 (1991).
38. E. Leithe, M. Mesnil, T. Aasen, The connexin 43 C-terminus: A tail of many tales. *Biochim Biophys Acta Biomembr* **1860**, 48-64 (2018).
39. T. Aasen *et al.*, Connexins in cancer: bridging the gap to the clinic. *Oncogene* **38**, 4429-4451 (2019).
40. D. Zhu, S. Caveney, G. M. Kidder, C. C. Naus, Transfection of C6 glioma cells with connexin 43 cDNA: analysis of expression, intercellular coupling, and cell proliferation. *Proc Natl Acad Sci U S A* **88**, 1883-1887 (1991).
41. R. P. Huang, M. Z. Hossain, A. Sehgal, A. L. Boynton, Reduced connexin43 expression in high-grade human brain glioma cells. *J Surg Oncol* **70**, 21-24 (1999).
42. R. P. Huang *et al.*, Reversion of the neoplastic phenotype of human glioblastoma cells by connexin 43 (cx43). *Cancer Res* **58**, 5089-5096 (1998).
43. P. R. Gielen *et al.*, Connexin43 confers Temozolomide resistance in human glioma cells by modulating the mitochondrial apoptosis pathway. *Neuropharmacology* **75**, 539-548 (2013).

44. J. H. Lin *et al.*, Connexin 43 enhances the adhesivity and mediates the invasion of malignant glioma cells. *J Neurosci* **22**, 4302-4311 (2002).

45. P. L. Sorgen *et al.*, Structural changes in the carboxyl terminus of the gap junction protein connexin43 indicates signaling between binding domains for c-Src and zonula occludens-1. *J Biol Chem* **279**, 54695-54701 (2004).

46. S. J. Parsons, J. T. Parsons, Src family kinases, key regulators of signal transduction. *Oncogene* **23**, 7906-7909 (2004).

47. M. Guarino, Src signaling in cancer invasion. *J Cell Physiol* **223**, 14-26 (2010).

48. E. L. Mayer, I. E. Krop, Advances in targeting SRC in the treatment of breast cancer and other solid malignancies. *Clin Cancer Res* **16**, 3526-3532 (2010).

49. S. Martellucci *et al.*, Src Family Kinases as Therapeutic Targets in Advanced Solid Tumors: What We Have Learned so Far. *Cancers (Basel)* **12**, (2020).

50. E. Redin *et al.*, SRC family kinase (SFK) inhibitor dasatinib improves the antitumor activity of anti-PD-1 in NSCLC models by inhibiting Treg cell conversion and proliferation. *J Immunother Cancer* **9**, (2021).

51. S. Zhang, D. Yu, Targeting Src family kinases in anti-cancer therapies: turning promise into triumph. *Trends Pharmacol Sci* **33**, 122-128 (2012).

52. X. Han *et al.*, The role of Src family kinases in growth and migration of glioma stem cells. *Int J Oncol* **45**, 302-310 (2014).

53. J. Du *et al.*, Bead-based profiling of tyrosine kinase phosphorylation identifies SRC as a potential target for glioblastoma therapy. *Nat Biotechnol* **27**, 77-83 (2009).

54. S. G. Pelaz, A. Tabernero, Src: coordinating metabolism in cancer. *Oncogene* **41**, 4917-4928 (2022).

55. M. S. Ahluwalia, J. de Groot, W. M. Liu, C. L. Gladson, Targeting SRC in glioblastoma tumors and brain metastases: rationale and preclinical studies. *Cancer Lett* **298**, 139-149 (2010).

56. C. Cirotti, C. Contadini, D. Barilà, SRC Kinase in Glioblastoma: News from an Old Acquaintance. *Cancers* **12**, 1558 (2020).

57. S. G. Pelaz, C. Ollauri-Ibáñez, C. Lillo, A. Tabernero, Impairment of Autophagic Flux Participates in the Antitumor Effects of TAT-Cx43. *Cancers (Basel)* **13**, (2021).

58. R. Roskoski, Src kinase regulation by phosphorylation and dephosphorylation. *Biochem Biophys Res Commun* **331**, 1-14 (2005).

59. M. Okada, S. Nada, Y. Yamanashi, T. Yamamoto, H. Nakagawa, CSK: a protein-tyrosine kinase involved in regulation of src family kinases. *J Biol Chem* **266**, 24249-24252 (1991).

60. S. Zhang *et al.*, Combating trastuzumab resistance by targeting SRC, a common node downstream of multiple resistance pathways. *Nat Med* **17**, 461-469 (2011).

61. A. González-Sánchez *et al.*, Connexin43 recruits PTEN and Csk to inhibit c-Src activity in glioma cells and astrocytes. *Oncotarget* **7**, 49819-49833 (2016).

62. S. Herrero-González *et al.*, Connexin43 inhibits the oncogenic activity of c-Src in C6 glioma cells. *Oncogene* **29**, 5712-5723 (2010).

63. E. Gangoso, C. Thirant, H. Chneiweiss, J. M. Medina, A. Tabernero, A cell-penetrating peptide based on the interaction between c-Src and connexin43 reverses glioma stem cell phenotype. *Cell Death Dis* **5**, e1023 (2014).

64. E. E. Mulkearns-Hubert *et al.*, Development of a Cx46 Targeting Strategy for Cancer Stem Cells. *Cell Rep* **27**, 1062-1072.e1065 (2019).

65. E. E. Mulkearns-Hubert *et al.*, Targeting NANOG and FAK via Cx26-derived cell-penetrating peptides in triple-negative breast cancer. *Mol Cancer Ther*, (2023).

66. S. F. Murphy *et al.*, Connexin 43 Inhibition Sensitizes Chemoresistant Glioblastoma Cells to Temozolomide. *Cancer Res* **76**, 139-149 (2016).

67. Q. Chen *et al.*, Carcinoma-astrocyte gap junctions promote brain metastasis by cGAMP transfer. *Nature* **533**, 493-498 (2016).

68. A. D. Frankel, C. O. Pabo, Cellular uptake of the tat protein from human immunodeficiency virus. *Cell* **55**, 1189-1193 (1988).

69. M. Jaraíz-Rodríguez *et al.*, A Short Region of Connexin43 Reduces Human Glioma Stem Cell Migration, Invasion, and Survival through Src, PTEN, and FAK. *Stem Cell Reports* **9**, 451-463 (2017).

70. S. G. Pelaz *et al.*, Targeting metabolic plasticity in glioma stem cells in vitro and in vivo through specific inhibition of c-Src by TAT-Cx43. *EBioMedicine* **62**, 103134 (2020).

71. L. García-Vicente *et al.*, Single-nucleus RNA sequencing provides insights into the GL261-GSC syngeneic mouse model of glioblastoma. *bioRxiv*, 2023.2010.2026.564166 (2023).

72. M. Jaraíz-Rodríguez *et al.*, Connexin43 peptide, TAT-Cx43266-283, selectively targets glioma cells, impairs malignant growth, and enhances survival in mouse models in vivo. *Neuro Oncol* **22**, 493-504 (2020).

73. S. M. Pollard *et al.*, Glioma stem cell lines expanded in adherent culture have tumor-specific phenotypes and are suitable for chemical and genetic screens. *Cell Stem Cell* **4**, 568-580 (2009).

74. L. P. Deleyrolle *et al.*, Evidence for label-retaining tumour-initiating cells

in human glioblastoma. *Brain* **134**, 1331-1343 (2011).

75. J. D. Lathia *et al.*, Direct in vivo evidence for tumor propagation by glioblastoma cancer stem cells. *PLoS One* **6**, e24807 (2011).

76. S. J. Sundar *et al.*, Three-dimensional organoid culture unveils resistance to clinical therapies in adult and pediatric glioblastoma. *Transl Oncol* **15**, 101251 (2022).

77. K. P. L. Bhat *et al.*, Mesenchymal differentiation mediated by NF-κB promotes radiation resistance in glioblastoma. *Cancer Cell* **24**, 331-346 (2013).

78. C. G. Hubert *et al.*, Genome-wide RNAi screens in human brain tumor isolates reveal a novel viability requirement for PHF5A. *Genes Dev* **27**, 1032-1045 (2013).

79. L. Yi *et al.*, Implantation of GL261 neurospheres into C57/BL6 mice: a more reliable syngeneic graft model for research on glioma-initiating cells. *Int J Oncol* **43**, 477-484 (2013).

80. E. Gangoso, C. Thirant, H. Chneiweiss, J. M. Medina, A. Tabernero, A cell-penetrating peptide based on the interaction between c-Src and connexin43 reverses glioma stem cell phenotype. *Cell Death & Disease* **5**, (2014).

81. A. Gonzalez-Sanchez *et al.*, Connexin43 recruits PTEN and Csk to inhibit c-Src activity in glioma cells and astrocytes. *Oncotarget* **7**, 49819-49833 (2016).

82. M. Jaraíz-Rodríguez *et al.*, Connexin43 Peptide, TAT-Cx43266-283, Selectively Targets Glioma Cells, Impairs Malignant Growth, and Enhances Survival in Mouse Models in Vivo. *Neuro-oncology* **22**, 493-504 (2020).

83. C. W. Brennan *et al.*, The somatic genomic landscape of glioblastoma. *Cell* **155**, 462-477 (2013).

84. E. Cerami *et al.*, The cBio cancer genomics portal: an open platform for exploring multidimensional cancer genomics data. *Cancer Discov* **2**, 401-404 (2012).

85. R. L. Bowman, Q. Wang, A. Carro, R. G. Verhaak, M. Squatrito, GlioVis data portal for visualization and analysis of brain tumor expression datasets. *Neuro Oncol* **19**, 139-141 (2017).

86. C. L. Maire, K. L. Ligon, Molecular pathologic diagnosis of epidermal growth factor receptor. *Neuro Oncol* **16 Suppl 8**, viii1-6 (2014).

87. F. B. Furnari, T. F. Cloughesy, W. K. Cavenee, P. S. Mischel, Heterogeneity of epidermal growth factor receptor signalling networks in glioblastoma. *Nat Rev Cancer* **15**, 302-310 (2015).

88. H. Xu *et al.*, Epidermal growth factor receptor in glioblastoma. *Oncol Lett* **14**, 512-516 (2017).

89. E. Eskilsson *et al.*, EGFRvIII mutations can emerge as late and heterogenous events in glioblastoma development and promote angiogenesis through

Src activation. *Neuro Oncol* **18**, 1644-1655 (2016).

90. A. Dhawan, V. S. K. Manem, G. Yeaney, J. D. Lathia, M. S. Ahluwalia, EGFR Pathway Expression Persists in Recurrent Glioblastoma Independent of Amplification Status. *Cancers (Basel)* **15**, (2023).

91. P. B. Dirks, Brain tumor stem cells: the cancer stem cell hypothesis writ large. *Mol Oncol* **4**, 420-430 (2010).

92. T. Goi *et al.*, An EGF receptor/Ral-GTPase signaling cascade regulates c-Src activity and substrate specificity. *EMBO J* **19**, 623-630 (2000).

93. S. Singh *et al.*, EGFR/Src/Akt signaling modulates Sox2 expression and self-renewal of stem-like side-population cells in non-small cell lung cancer. *Mol Cancer* **11**, 73 (2012).

94. M. E. Irwin, N. Bohin, J. L. Boerner, Src family kinases mediate epidermal growth factor receptor signaling from lipid rafts in breast cancer cells. *Cancer Biol Ther* **12**, 718-726 (2011).

95. J. S. Biscardi *et al.*, c-Src-mediated phosphorylation of the epidermal growth factor receptor on Tyr845 and Tyr1101 is associated with modulation of receptor function. *J Biol Chem* **274**, 8335-8343 (1999).

96. D. R. Stover, M. Becker, J. Liebetanz, N. B. Lydon, Src phosphorylation of the epidermal growth factor receptor at novel sites mediates receptor interaction with Src and P85 alpha. *J Biol Chem* **270**, 15591-15597 (1995).

97. K. Sato, A. Sato, M. Aoto, Y. Fukami, Site-specific association of c-Src with epidermal growth factor receptor in A431 cells. *Biochem Biophys Res Commun* **210**, 844-851 (1995).

98. A. N. Cvrljevic *et al.*, Activation of Src induces mitochondrial localisation of de2-7EGFR (EGFRvIII) in glioma cells: implications for glucose metabolism. *J Cell Sci* **124**, 2938-2950 (2011).

99. M. C. Maa, T. H. Leu, D. J. McCarley, R. C. Schatzman, S. J. Parsons, Potentiation of epidermal growth factor receptor-mediated oncogenesis by c-Src: implications for the etiology of multiple human cancers. *Proc Natl Acad Sci U S A* **92**, 6981-6985 (1995).

100. D. A. Tice, J. S. Biscardi, A. L. Nickles, S. J. Parsons, Mechanism of biological synergy between cellular Src and epidermal growth factor receptor. *Proc Natl Acad Sci U S A* **96**, 1415-1420 (1999).

101. M. Dimri *et al.*, Modeling breast cancer-associated c-Src and EGFR overexpression in human MECs: c-Src and EGFR cooperatively promote aberrant three-dimensional acinar structure and invasive behavior. *Cancer Res* **67**, 4164-4172 (2007).

102. R. S. Kenchappa *et al.*, Activation of STAT3 through combined SRC and EGFR signaling drives resistance to a mitotic kinesin inhibitor in glioblastoma. *Cell Rep* **39**, 110991 (2022).

103. R. Sachdeva *et al.*, BMP signaling mediates glioma stem cell quiescence and confers treatment resistance in glioblastoma. *Sci Rep* **9**, 14569 (2019).

104. K. M. Ferguson *et al.*, Lrig1 regulates the balance between proliferation and quiescence in glioblastoma stem cells. *Front Cell Dev Biol* **10**, 983097 (2022).

105. M. Marqués-Torrejón *et al.*, LRIG1 is a gatekeeper to exit from quiescence in adult neural stem cells. *Nat Commun* **12**, 2594 (2021).

106. L. Curtin *et al.*, Shape matters: morphological metrics of glioblastoma imaging abnormalities as biomarkers of prognosis. *Sci Rep* **11**, 23202 (2021).

107. C. Horbinski, T. Berger, R. J. Packer, P. Y. Wen, Clinical implications of the 2021 edition of the WHO classification of central nervous system tumours. *Nat Rev Neurol* **18**, 515-529 (2022).

108. J. F. Cloutier, A. Veillette, Cooperative inhibition of T-cell antigen receptor signaling by a complex between a kinase and a phosphatase. *J Exp Med* **189**, 111-121 (1999).

109. B. M. Chung *et al.*, The role of cooperativity with Src in oncogenic transformation mediated by non-small cell lung cancer-associated EGF receptor mutants. *Oncogene* **28**, 1821-1832 (2009).

110. M. J. van den Bent *et al.*, Randomized phase II trial of erlotinib versus temozolomide or carmustine in recurrent glioblastoma: EORTC brain tumor group study 26034. *J Clin Oncol* **27**, 1268-1274 (2009).

111. L. P. Stabile *et al.*, c-Src activation mediates erlotinib resistance in head and neck cancer by stimulating c-Met. *Clin Cancer Res* **19**, 380-392 (2013).

112. B. C. Creelan *et al.*, Phase 1 trial of dasatinib combined with afatinib for epidermal growth factor receptor-(EGFR-) mutated lung cancer with acquired tyrosine kinase inhibitor (TKI) resistance. *Br J Cancer* **120**, 791-796 (2019).

113. D. A. Reardon *et al.*, Phase 1 trial of dasatinib plus erlotinib in adults with recurrent malignant glioma. *J Neurooncol* **108**, 499-506 (2012).

114. Y. Li *et al.*, Copper improves the anti-angiogenic activity of disulfiram through the EGFR/Src/VEGF pathway in gliomas. *Cancer Lett* **369**, 86-96 (2015).

115. C. Ollauri-Ibáñez, B. Ayuso-Íñigo, M. Pericacho, Hot and Cold Tumors: Is Endoglin (CD105) a Potential Target for Vessel Normalization? *Cancers (Basel)* **13**, (2021).

116. P. Karschnia *et al.*, Prognostic validation of a new classification system for extent of resection in glioblastoma: A report of the RANO resect group. *Neuro Oncol* **25**, 940-954 (2023).

117. T. J. Brown *et al.*, Association of the Extent of Resection With Survival in Glioblastoma: A Systematic Review and Meta-analysis. *JAMA Oncol* **2**, 1460-1469 (2016).

118. F. Gessler *et al.*, Surgery for Glioblastoma in Light of Molecular Markers: Impact of Resection and MGMT Promoter Methylation in Newly Diagnosed IDH-1 Wild-Type Glioblastomas. *Neurosurgery* **84**, 190-197 (2019).

119. A. M. Molinaro *et al.*, Association of Maximal Extent of Resection of Contrast-Enhanced and Non-Contrast-Enhanced Tumor With Survival Within Molecular Subgroups of Patients With Newly Diagnosed Glioblastoma. *JAMA Oncol* **6**, 495-503 (2020).

120. Y. M. Li, D. Suki, K. Hess, R. Sawaya, The influence of maximum safe resection of glioblastoma on survival in 1229 patients: Can we do better than gross-total resection? *J Neurosurg* **124**, 977-988 (2016).

121. F. Seker-Polat, N. Pinarbasi Degirmenci, I. Solaroglu, T. Bagci-Onder, Tumor Cell Infiltration into the Brain in Glioblastoma: From Mechanisms to Clinical Perspectives. *Cancers (Basel)* **14**, (2022).

122. O. Okolie *et al.*, Reactive astrocytes potentiate tumor aggressiveness in a murine glioma resection and recurrence model. *Neuro Oncol* **18**, 1622-1633 (2016).

123. A. M. Knudsen *et al.*, Surgical resection of glioblastomas induces pleiotrophin-mediated self-renewal of glioblastoma stem cells in recurrent tumors. *Neuro Oncol* **24**, 1074-1087 (2022).

124. E. L. Abhold *et al.*, EGFR kinase promotes acquisition of stem cell-like properties: a potential therapeutic target in head and neck squamous cell carcinoma stem cells. *PLoS One* **7**, e32459 (2012).

125. M. Pudełek *et al.*, Epidermal Growth Factor (EGF) Augments the Invasive Potential of Human Glioblastoma Multiforme Cells via the Activation of Collaborative EGFR/ROS-Dependent Signaling. *Int J Mol Sci* **21**, (2020).

126. Y. Rong, D. L. Durden, E. G. Van Meir, D. J. Brat, 'Pseudopalisading' necrosis in glioblastoma: a familiar morphologic feature that links vascular pathology, hypoxia, and angiogenesis. *J Neuropathol Exp Neurol* **65**, 529-539 (2006).

127. A. Hatoum, R. Mohammed, O. Zakieh, The unique invasiveness of glioblastoma and possible drug targets on extracellular matrix. *Cancer Manag Res* **11**, 1843-1855 (2019).

128. S. Das, P. A. Marsden, Angiogenesis in glioblastoma. *N Engl J Med* **369**, 1561-1563 (2013).

129. G. Seano, R. K. Jain, Vessel co-option in glioblastoma: emerging insights and opportunities. *Angiogenesis* **23**, 9-16 (2020).

130. A. Comba *et al.*, Spatiotemporal analysis of glioma heterogeneity reveals COL1A1 as an actionable target to disrupt tumor progression. *Nat Commun* **13**, 3606 (2022).

131. V. Genoud *et al.*, Responsiveness to anti-PD-1 and anti-CTLA-4 immune checkpoint blockade in SB28 and GL261 mouse glioma models. *Oncoimmunology* **7**, e1501137 (2018).

132. E. F. Simonds *et al.*, Deep immune profiling reveals targetable mechanisms of immune evasion in immune checkpoint inhibitor-refractory glioblastoma. *J Immunother Cancer* **9**, (2021).

133. A. F. Haddad *et al.*, Mouse models of glioblastoma for the evaluation of novel therapeutic strategies. *Neurooncol Adv* **3**, vdab100 (2021).

134. C. Liu *et al.*, The Interaction between Cancer Stem Cell Marker CD133 and Src Protein Promotes Focal Adhesion Kinase (FAK) Phosphorylation and Cell Migration. *J Biol Chem* **291**, 15540-15550 (2016).

135. C. V. Lund *et al.*, Reduced glioma infiltration in Src-deficient mice. *J Neurooncol* **78**, 19-29 (2006).

136. H. Eom *et al.*, MerTK mediates STAT3-KRAS/SRC-signaling axis for glioma stem cell maintenance. *Artif Cells Nanomed Biotechnol* **46**, 87-95 (2018).

137. Y. Zhao *et al.*, Recent advances in drug delivery systems for targeting brain tumors. *Drug Deliv* **30**, 1-18 (2023).

138. F. Marcucci, A. Corti, A. J. M. Ferreri, Breaching the Blood-Brain Tumor Barrier for Tumor Therapy. *Cancers (Basel)* **13**, (2021).

139. L. S. Ashby, K. A. Smith, B. Stea, Gliadel wafer implantation combined with standard radiotherapy and concurrent followed by adjuvant temozolomide for treatment of newly diagnosed high-grade glioma: a systematic literature review. *World J Surg Oncol* **14**, 225 (2016).

140. N. B. T. Society. PDF link: https://braintumor.wpenginepowered.com/wp-content/uploads/2022/08/2017_NBTS_CurrentTreatmentOptions_083017.pdf

141. C. Chen *et al.*, Intracavity generation of glioma stem cell-specific CAR macrophages primes locoregional immunity for postoperative glioblastoma therapy. *Sci Transl Med* **14**, eabn1128 (2022).

142. A. P. Becker, B. E. Sells, S. J. Haque, A. Chakravarti, Tumor Heterogeneity in Glioblastomas: From Light Microscopy to Molecular Pathology. *Cancers (Basel)* **13**, (2021).

143. K. Yang *et al.*, Glioma targeted therapy: insight into future of molecular approaches. *Mol Cancer* **21**, 39 (2022).

144. J. V. R. Cruz *et al.*, Obstacles to Glioblastoma Treatment Two

Decades after Temozolomide. *Cancers (Basel)* **14**, (2022).

145. A. M. Sonabend *et al.*, Repeated blood-brain barrier opening with an implantable ultrasound device for delivery of albumin-bound paclitaxel in patients with recurrent glioblastoma: a phase 1 trial. *Lancet Oncol* **24**, 509-522 (2023).

146. M. Alieva *et al.*, Preventing inflammation inhibits biopsy-mediated changes in tumor cell behavior. *Sci Rep* **7**, 7529 (2017).

147. S. Hingtgen *et al.*, Real-time multi-modality imaging of glioblastoma tumor resection and recurrence. *J Neurooncol* **111**, 153-161 (2013).

148. S. Weil *et al.*, Tumor microtubes convey resistance to surgical lesions and chemotherapy in gliomas. *Neuro Oncol* **19**, 1316-1326 (2017).

149. F. Akter *et al.*, Pre-clinical tumor models of primary brain tumors: Challenges and opportunities. *Biochim Biophys Acta Rev Cancer* **1875**, 188458 (2021).

150. S. H. Choi *et al.*, Tumor Resection Recruits Effector T Cells and Boosts Therapeutic Efficacy of Encapsulated Stem Cells Expressing IFNβ in Glioblastomas. *Clin Cancer Res* **23**, 7047-7058 (2017).

151. C. Garcia-Diaz *et al.*, Glioblastoma cell fate is differentially regulated by the microenvironments of the tumor bulk and infiltrative margin. *Cell Rep* **42**, 112472 (2023).